

**Investigation of Processing Conditions and Viscoelastic Properties on Frictional Sliding
Behavior of Unidirectional Carbon Fiber Epoxy Prepreg**

Kathleen J. Chan

Thesis submitted to the faculty of the Virginia Polytechnic Institute and State University in
partial fulfillment of the requirements for the degree of

Master of Science

In

Chemical Engineering

Michael J. Bortner, Chair

David A. Dillard

Richey M. Davis

October 22, 2018

Blacksburg, VA

Keywords: Fiber reinforced polymer composites, prepreg, tool-ply friction, rheometer,
composite forming process, time-temperature transformation

Investigation of Processing Conditions and Viscoelastic Properties on Frictional Sliding Behavior of Unidirectional Carbon Fiber Epoxy Prepreg

Kathleen J. Chan

ACADEMIC ABSTRACT

The quality of continuous fiber reinforced polymer matrix composite parts and structures depends strongly on the friction during the composite forming process. The two major types of friction that cause deformations during this process are ply-ply friction and tool-ply friction. One of the challenges in the composite forming process is the occurrence of wrinkling and shape distortion of the fabric caused by the surface differences between the forming tool and surface of the laminate. Frictional measurements of composites can vary widely depending on processing parameters, measurement technique, and instruments used.

In this study, a commercial rheometer was used to evaluate tool-ply friction of unidirectional carbon fiber epoxy prepreg at various contact pressures, temperatures and sliding velocities. Viscoelastic properties such as the complex viscosity (η^*), storage modulus (G'), loss modulus (G''), and loss factor ($\tan \delta$) were used to determine the critical transition events (such as gelation) during cure. An understanding of changes in viscoelastic properties as a function of time, temperature, and cure provides insight for establishing a suitable processing range for compression forming of prepreg systems.

Surface imaging results were coupled with rheological results to qualitatively examine the effects of processing parameters on prepreg distortions. Changes in gap height over the measurement interval qualitatively describe the changes in contact area and contact mechanisms between the tool-ply surfaces. The results indicate that friction behavior of the prepreg system is a contribution of adhesive and frictional forces, where increase in viscosity, reduction in gap height, and cure of the sample correlate to higher friction values.

Investigation of Processing Conditions and Viscoelastic Properties on Frictional Sliding Behavior of Unidirectional Carbon Fiber Epoxy Prepreg

Kathleen J. Chan

GENERAL AUDIENCE ABSTRACT

The quality of composite parts and structures depends strongly on the friction present during the composite forming process. One of the major challenges in the forming process is the occurrence of wrinkling and shape distortions of the fabric caused by the surface differences between the forming tool and material. The presence of these defects can compromise the final material property and lead to failure when in use. Frictional measurements of composites can vary widely depending on processing parameters, measurement technique, and instruments used. The extent of interaction between the tool and surface of the material depends on the tooling height, and by extension, contact area, which cannot easily be monitored with traditional test designs.

A commercial rheometer was used in this study to evaluate tool-ply friction of unidirectional carbon fiber epoxy prepreg at various contact pressures, temperatures, and sliding velocities. Gap height and torque were monitored to provide information on the frictional dependence of processing parameters. In addition, surface-imaging results were coupled with rheological results to examine the relationship between friction and fiber distortions. The understanding of changes in material property with respect to the tooling process is the key to optimizing the composite forming process.

ACKNOWLEDGEMENTS

I would first like to express my gratitude to my advisor, Dr. Michael Bortner, for his continuous support, patience, guidance, and for providing me the opportunity to work in his research group these past few years. I would also like to thank my committee members: Dr. David Dillard for his feedback and support on the project, and Dr. Richey Davis for serving on my committee.

I would like to thank Dr. Jack Lesko, Dr. Nicole Sanderlin, and Christine Burgoyne for their advice on graduate school and for giving me the amazing opportunity to participate in the International Research Experience for Students (IRES) program at the University of Nottingham in Nottingham, UK. I would also like to acknowledge the financial support from NSF for the IRES program.

I would like to thank the Department of Chemical Engineering, the Macromolecules and Interfaces Institute at Virginia Tech, and the Department of Mechanical, Materials and Manufacturing at the University of Nottingham for providing the facilities and opportunities to conduct this research.

My sincere thanks goes to Dr. Davide De Focatiis at the University of the Nottingham for his insightful comments and guidance on the project. A special thanks to his lab group and students, Vinotharan Annarasa and Matthew Elsmore, for their advice and help during my stay, for letting me know that teatime IS mandatory, and for showing me that crumpets are more than just fluffy pancakes.

It is my pleasure to thank my colleagues: Cailean Pritchard, Eric Gilmer, Arit Das, Jake Fallon, Bradley Sutliff, and David Anderegg for their motivation, friendship, and support through this journey.

Finally, I would like to thank my parents for their love and sacrifice, and my siblings for challenging me to become a better person. Special thanks to my husband, Stephen O'Connor, for giving me the strength and encouragement when I needed it the most.

TABLE OF CONTENTS

CHAPTER 1	1
INTRODUCTION	1
1.1 Motivation	1
1.2 Research Objectives	2
CHAPTER 2	3
BACKGROUND AND LITERATURE REVIEW	3
2.1 Fiber Reinforced Polymer Composites	3
2.1.1 Fiber Materials and Arrangements	5
2.1.2 Matrix Materials	6
2.2 Composite Forming Processes	8
2.2.1 Manual and Automated Layup Process	8
2.2.2 Compression Molding	9
2.3 Tool-Ply Friction	10
2.3.1 Effects of Testing Conditions on Tool-ply friction	13
2.3.2 Effects of Fiber and Resin on Tool-Ply Friction	14
2.3.3 Rheological Characterization of Tool-Ply Friction	16
2.4 Viscoelastic Properties of a Curing Thermoset	17
CHAPTER 3	20
MATERIALS AND METHODS	20
3.1 Materials	20
3.2 Equipment	21
3.2.1 Torsional Rheometer	21
3.2.2 Imaging	23
3.3 Methodology	23
3.3.1 Sample Preparation	23
3.3.2 Sample Heating	24
3.3.3 Viscoelastic and Cure Analysis	24
3.3.3.1 Determining the Linear Viscoelastic Region	24
3.3.3.2 Viscoelastic Measurements	25
3.3.3.3 Effects of Heating Rate on Minimum Viscosity	25
3.3.3.4 Effects of Temperature on Resin Staging	26

3.3.3.5 Time Temperature Transformation (TTT) Study	26
3.3.4 Tool-ply Friction Measurements	27
3.3.4.1 Friction Calculations	28
CHAPTER 4	31
EXPERIMENTAL RESULTS AND DISCUSSION	31
4.1 Rheological Analysis of Viscoelastic and Cure Behavior	31
4.1.1 General Viscoelastic Behavior	31
4.1.3 Effects of Temperature on Resin Staging	41
4.1.4 Time Temperature Transformation (TTT)	43
4.2 Tool-Ply Friction	50
4.2.1 Influence of Temperature on Tool-Ply Friction	50
4.2.1.1 Data Repeatability	52
4.2.2 Influence of Velocity on Tool-Ply Friction	54
4.2.3 Influence of Pressure on Tool-Ply Friction	55
4.2.4 Influence of Temperature on Sample Deformation	57
4.2.5 Influence of Resin Staging on Tool-Ply Friction	58
4.3 Description of Overall Friction behavior in Thermosetting Prepreg Systems	61
4.3.1 Proposed Friction Map	62
CHAPTER 5	66
CONCLUSIONS AND FUTURE RECOMMENDATIONS	66
5.1 Conclusions	66
5.2 Recommendation for Future Studies	69
REFERENCES	70
Appendix A	75
Determination of Linear Viscoelastic Region and Effects of Sample Shape and Adhesive Type on Rheological Properties of HexPly M77 UD Prepreg	75
A.1 Material and Methods	75
A.1.2 Sample Preparation	75
A.1.3 Rheological Measurements	75
A.2 Results and Discussion	76
A.2.2 Effect of Sample Adhesive Type on Rheological Properties	78
A.3 Conclusion	80
Appendix B	81

Effects of Surface Roughness and Dwell time on Frictional Sliding Tests	81
B.1 Material and Methods	81
B.1.1 Material	81
B.1.2 Sample Preparation	82
B.1.3 Rheological measurements	82
B.1.4 Sample staging	82
B.2 Results and Discussion	82
B.2.1 Repeatability of Uncured Samples.....	82
B.2.2 Repeatability of Cured samples	85
B.3 Conclusion	86

LIST OF FIGURES

Figure 1. Comparison of strength-to-density ratio of various materials (Ashby plot). (■) Engineering ceramics, (□) Engineering/FRP composites, (▣) Engineering alloys.....	4
Figure 2. Common fiber arrangements in FRPC (a.)continuous fiber, (b.) discontinuous fiber. ...	5
Figure 3. schematic of network formation of thermosetting polymer (a) A-stage resin with unreacted monomers, (b) B-stage resin with monomers and higher molecular weight oligomers, (c) gelation, onset of 3-D network formation (d) C-stage with fully cured resin system	7
Figure 4. Simplified schematic of the ATL process	8
Figure 5. Interfacial (a) and cohesive (b) failure mode observed during peel-ply test.....	9
Figure 6. Overall (top) and detailed stages (bottom) of the compression molding process	10
Figure 7. Schematic of pull-out (L) and pull-through (R) method	11
Figure 8. Generalized Stribeck curve with three regions. 1.) Boundary lubrication (BL) 2.) mixed lubrication (ML) and 3) elasto-hydrodynamic lubrication ((E)HL)	12
Figure 9. Generalized isothermal time-temperature transformation (TTT) cure diagram for a thermosetting system	17
Figure 10. Anton Parr MCR 302 Rheometer with CTD 450 convection temperature chamber ..	21
Figure 11. Modified plate geometry with 1mm annulus.....	23
Figure 12. Prepreg fiber orientation in rheometer	24
Figure 13. Schematic diagram of parallel plate rheometer plates (left), wedged sample in cylindrical coordinates (middle), and elemental area of a specimen (right).....	28
Figure 14 . Sample friction plot used to determine μ_s and μ_k	30
Figure 15. Typical cure diagram of viscoelastic behaviors obtained through rheology	32
Figure 16. Evolution of complex viscosity over time at various heating rates.....	34
Figure 17. Viscosity profile of the neat epoxy resin system (Hexply® M77 product data sheet ⁴⁷) compared to M77 prepreg (experimental) at a heating rate of $5^\circ\text{C}\cdot\text{min}^{-1}$	35
Figure 18. Changes in complex viscosity and gap height over the measurement interval	37
Figure 19. Top view of as received prepreg (HexPly M77/38%/UD300/50K) with varied resin coverage across surface (sample size 120 x 90 mm)	40
Figure 20. Effect of temperature on resin staging.....	42
Figure 21. Critical gelation time at various cure temperatures determined by Arrhenius fit	46
Figure 22. Modified TTT diagram.....	48
Figure 23. Frictional force vs. deflection angle at three temperatures (angular velocity 1mrad/s, normal force of 5N ($6.63\cdot 10^4$ Pa)) *values reported from second iteration (with 200s dwell time)	51
Figure 24. Changes in static and kinetic friction values measured various iterations at 20°C, 40°C, 60°C (rotational velocity of 100mrad/s and normal force of 5N (contact pressure of $6.63\cdot 10^4$ Pa))	53
Figure 25. Frictional force vs. angular velocity for 40°C, 60°C samples (normal force of 5N) *values reported from second iteration (with 200s dwell time)	54
Figure 26. Frictional force at normal forces of 0.5, 2, 5N (contact pressure of $6.63\cdot 10^3$, $2.65\cdot 10^4$, $6.63\cdot 10^4$ Pa, respectively) (40°C, angular velocity $10\text{mrad}\cdot\text{s}^{-1}$) *values reported from second iteration (with 200s dwell time).....	56

Figure 27. Top view and microscope images of samples after frictional sliding tests	57
Figure 28. Frictional force vs. deflection angle from α 0.06 to 0.16. (90°C, angular velocity 10mrad/s, normal force of 5N ($1.02 \cdot 10^4$ Pa), rest time of 291s per interval)	59
Figure 29. Frictional force vs. deflection angle from α 0.16 to 0.69. (90°C, angular velocity $10\text{mrad} \cdot \text{s}^{-1}$, normal force of 5N ($1.02 \cdot 10^4$ Pa), rest time of 291s per interval).....	60
Figure 30. Top view of cured prepreg after frictional sliding experiment.....	61
Figure 31. Proposed frictional sliding map.....	63

LIST OF TABLES

Table 1. Cure cycle of HexPly® M77 epoxy resin (obtained from HexPly datasheet) ⁴⁷	20
Table 2. Process limitations of Anton Parr MCR 302 rheometer fitted with CRD 450 heating chamber.....	22
Table 3. Contact pressure range of plate versus modified annulus geometry	23
Table 4. Test parameters for frictional sliding tests below 80°C.....	28
Table 5. Corresponding processing parameters at the minimum viscosity point for various heating rates	34
Table 6. Onset of increase in complex viscosity at various temperatures (“critical gap height region”)	38
Table 7. Time required to reach viscosity plateau region (“steady-state gap height region”).....	38
Table 8. Degree of conversion at various cure temperatures.....	42
Table 9. Average $T_{g,sub}$ values of 3 samples heated at 10°C/min from 20°C, 1hz, and 0.05% strain	43
Table 10. Gel times determined at the point at which viscosity rises to infinity (0.05 strain %, normal force 5N, 1hz).....	44
Table 11. Gel times determined with at which $\tan \delta$ drops suddenly (0.05 strain %, normal force 5N, 1hz).....	44
Table 12. Corresponding parameters for determining gelation through Arrhenius fit	46
Table 13. t_{vit} and relevant viscoelastic parameters determined various temperatures (0.05 strain %, normal force 5N, 1hz).....	47
Table 14. t_{cure} and relevant viscoelastic parameters determined various temperatures (0.05 strain %, normal force 5N, 1hz).....	48
Table 15. Corresponding parameters for the modified TTT diagram.....	49
Table 16. Viscoelastic properties measured from (1) high gap samples- SAOS at 0.05% strain, 1hz, heating rate of 10°C to 90°C (2) low gap samples- SAOS at 0.05% stain, 1hz, heating rate 10°C from 20°C to 40 or 60°C	51
Table 17. Time required to reach steady state gap height at various temperatures for frictional sliding measurements.....	53
Table 18. Summary of experimental results from various techniques.....	58

CHAPTER 1

INTRODUCTION

1.1 Motivation

Advanced composite materials, such as fiber reinforced polymer composites (FRPC), can be found in the aircraft, automotive, marine, and aerospace applications, as well as in consumer products such as canoes and tennis rackets.¹ Compared to metal and ceramic composites, FRPC can exhibit superior material properties such as higher stiffness, low density, tailored electrical and thermal conductivity, superior fatigue life, and corrosion resistance.¹ One of the benefits in using FRPC is the versatility in shapes and designs offered depending on the fiber and resin combination.² For example, reduction in weave density allows for superior drapability, while the addition of curing agents can reduce the curing time from hours to minutes.³ While this allows for flexibility in design, it also dramatically reduces the ability for generalizing the processing parameters, as slight changes in the material formulation require different processing parameters in order to achieve optimal properties in the final product. The use of FRPC is limited due to processing cost and other challenges. Defects in composite materials include wrinkling and shape distortion caused by the friction between the tool and the surface of the polymer material. An understanding of the relationship between material property and the tooling process is the key to optimizing the composite forming process.¹

Considerable efforts are put forth to develop models to predict tool-ply friction with respect to processing parameters such as forming temperature, pressure, and velocity.⁴ However, deviations in friction mechanisms are observed due to changes in the bulk viscoelastic behavior during processing. A challenge with traditional pull out and pull through methods is that they are often time-intensive and results are limited to specific equipments.⁵ Although alternative

methods of studying prepreg friction have been developed with commercial rheometers, limited experiments have been conducted to directly examine the effects of changes in viscoelastic properties during processing to support deviations observed in friction measurements.

1.2 Research Objectives

The main objective of this thesis is to broaden the understanding of the interfacial friction phenomena relevant to the composite forming process by:

- 1.) Investigating methodologies for consistent measurements of tool-ply friction with a commercial rheometer
- 2.) Establishing a relationship between viscoelastic state of prepreg material on the tool-ply friction of FRPC

The first goal is to determine the viscoelastic properties of the prepreg sample in its as received state. As mentioned above, the material properties of a system can vary widely depending on the fiber weave and epoxy formulation. The presence of the fiber can significantly affect the bulk viscoelastic behavior compared to the neat resin system.⁶ A commercial rheometer was used to study the changes in viscoelastic properties as a function of time and temperature.

The second goal is to characterize tool-ply friction of the forming process. A commercial rheometer was used to study the tool-ply friction at various sliding velocities, pressures, temperatures, and resin staging. The effect of resin staging on tool-friction is a particularly important parameter to consider in the forming process, as network formation and resin viscosity increases dramatically over the staging interval up to the gel point, which could alter the friction mechanism of the system.

CHAPTER 2

BACKGROUND AND LITERATURE REVIEW

2.1 Fiber Reinforced Polymer Composites

A composite material is a combination of two or more different materials that produces unique properties when combined. Fiber reinforced polymer composites (FRPC) are composed of fibers – such as fiberglass, carbon, nylon, and polyester – bonded by a thermosetting or thermoplastic polymer matrix. The fibers typically have high strength and modulus that can withstand stresses in the longitudinal direction of the load. The polymer matrix binds the material, which allows for further load/stress distribution and offers thermal, chemical, and environmental resistance that increases the overall fracture toughness and damage tolerance of the system.^{1,2,7,8}

The use of FRPC can be found in aircraft, automotive, marine, and aerospace applications, as well as in consumer products such as skis and tennis rackets.¹ One of the main benefits of FRPC is the high strength-to-weight ratio as compared to other engineering materials, such as metal or ceramics.⁹ A comparison of the strength-to-density ratio of various materials is shown in the Ashby plot in Figure 1 .

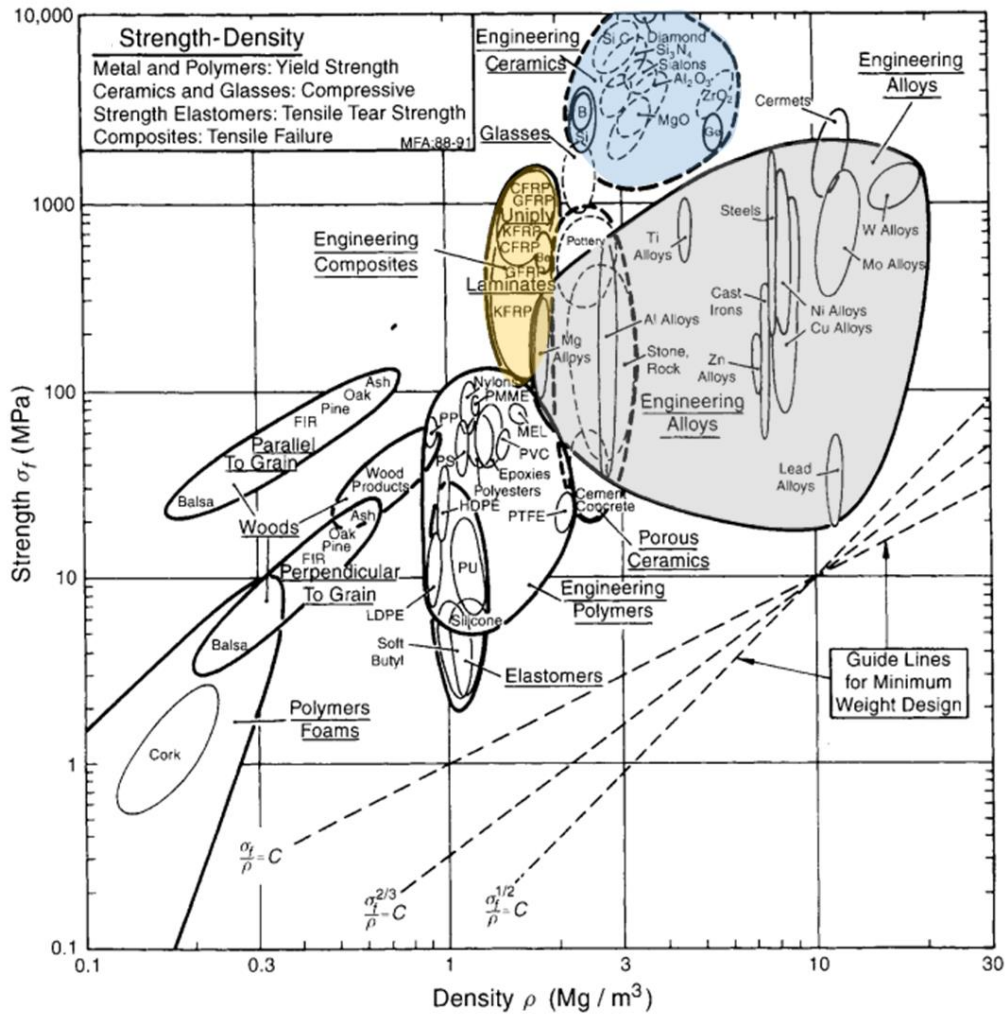


Figure 1. Comparison of strength-to-density ratio of various materials (Ashby plot).⁹ (■) Engineering ceramics, (□) Engineering/FRP composites, (□) Engineering alloys.

The high strength-to-weight ratio of FRPC is particularly advantageous in aeronautical application as weight reduction is proportional to fuel efficiency.¹⁰ For example, the switch from aluminum to 50% composite material in the Boeing 787 Dreamliner allowed a weight reduction of 20%, improving the fuel efficiency without sacrificing performance.¹ Another benefit in using FRPC is the flexibility for formation of more complex shapes and designs that are not traditionally available when utilizing ceramic or metal composites.¹⁰

2.1.1 Fiber Materials and Arrangement

In FRPC, the fiber is the primary reinforcing component that provides the strength and stiffness of the system.^{1,3,10-13} The mechanical properties are dependent on fiber type and arrangement. Common fibers used in FRPC are carbon, aramid, and fiberglass.^{3,12,13} The specific fiber used is dependent on the material application and costs. For example, fiberglass is commonly used due to the low material costs, while carbon-fiber is used in high-strength applications.^{1,10} There are two major fiber arrangement types: (1) continuous fibers, which are composed of long fibers aligned together and can be constructed into woven or knitted fabrics (Figure 2 (a)); and (2) discontinuous fibers, which are composed of shorter strands of fibers in either chopped or matted form in random orientations (Figure 2(b)).^{11,12}

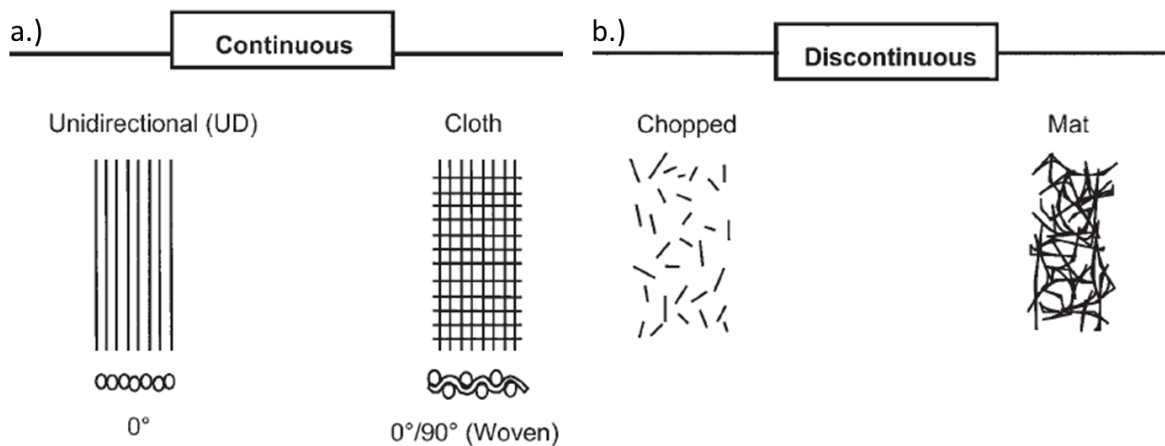


Figure 2. Common fiber arrangements in FRPC (a.) continuous fiber, (b.) discontinuous fiber.¹²

The reinforcement offered by the fiber is dependent on the orientation and length-to-diameter ratio (or aspect ratio). Continuous fibers typically offer much higher strength and stiffness in the direction of the load, due to fiber alignment and high aspect ratio, whereas discontinuous fibers offer lower strength and stiffness, due to the random fiber alignment. It should be noted that continuous fibers are generally limited to high performance applications due to higher production costs and longer production times.^{11,13,14} While both continuous and discontinuous fiber

reinforcement types are of significant importance in FRPC, this study is focused on processing of unidirectional carbon fiber reinforced composites.

2.1.2 Matrix Materials

The main purpose of the polymer matrix is to bind the fibers and to offer thermal, chemical, and environmental resistance for the system.^{1,2,7,8} The two main types of polymer resin used in FRPC are thermoplastic and thermosetting polymers.¹⁵ Common thermosetting polymer resins are polyesters, epoxies, phenolics, bismaleimides, polyimides and benzoxazines. Resin choice is typically dependent on cost and performance requirements. For example, bismaleimides and polyimides are typically used in applications that require high temperature resistance, while epoxies are typically used in processes that require high mechanical performance.^{2,7,8} One of the benefits of using polymer resin systems is the versatility in the material properties through the addition of different additive and fillers. For example, polymercaptan/epoxy systems can be rapidly cured in less than 10 minutes at low temperatures compared to a cure time of hours for neat epoxy systems.³ While the many resin formulations and fiber styles allows for flexibility in design, they also dramatically reduce the ability for generalizing the processing parameters required for the composite forming process.⁴

As the material used in this study is an epoxy-based thermosetting composite, the discussion will be focused on processing of thermosetting composites. A schematic of the structure formation of thermosetting polymer is shown in Figure 3.

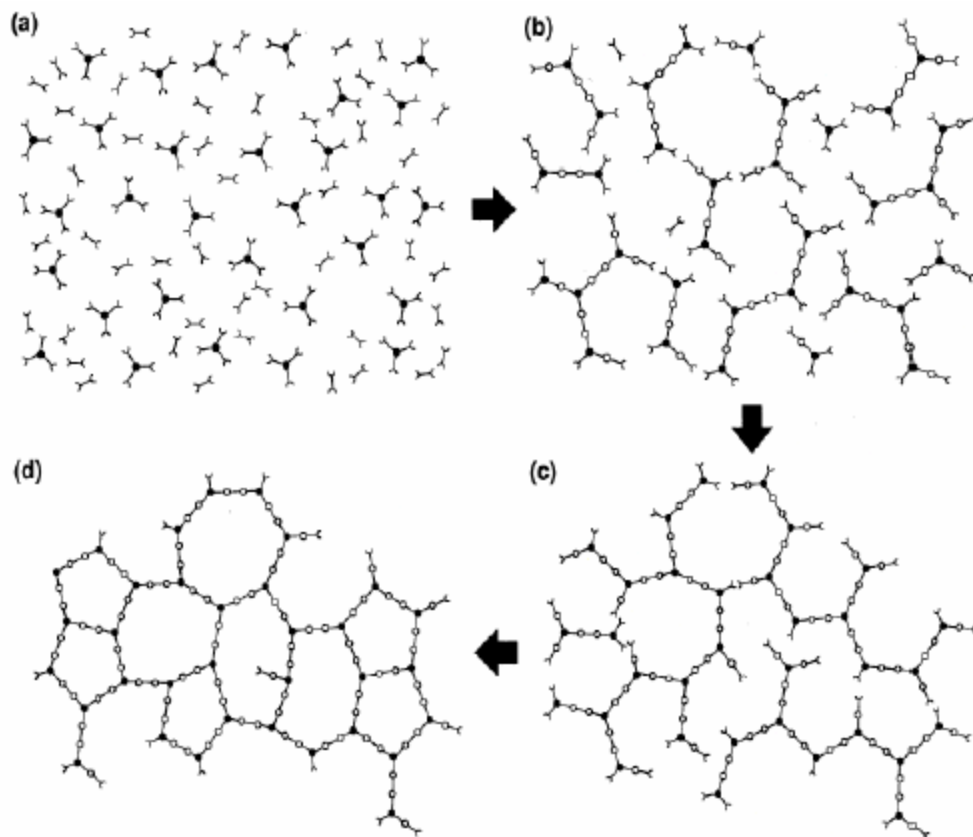


Figure 3. schematic of network formation of thermosetting polymer (a) A-stage resin with unreacted monomers, (b) B-stage resin with monomers and higher molecular weight oligomers, (c) gelation, onset of 3-D network formation (d) C-stage with fully cured resin system.¹⁶

During the initial stages of processing (A-stage) the material contains uncrosslinked linear and/or branched monomers. The material is characterized by low viscosity and is formable with minimal input of heat and pressure. In the B-stage, the system contains higher molecular weight oligomers due to covalent bond-formation between the monomers. The material is characterized with higher viscosity. Fibers are typically impregnated with A-stage resin, and partially cured to B-stage to promote ease of handling and processing.¹⁰ With increase in time and temperature, the material structure continues to build up to the gelation point, followed by crosslinking to form an insoluble 3-D network structure with solid-like characteristics (C-stage). The strength

and final properties are highly dependent on the chemistry of the polymer, combined with the time, temperature and pressure at which the curing reaction is conducted.^{8,16}

2.2 Composite Forming Processes

One of the most popular materials used in the industry is called prepreg, where the carbon fiber is “pre-impregnated” with A-stage resin and partially cured to B-stage to promote ease of handling and processing.¹⁰ While a wide variety of manufacturing processes are available for manufacturing of FRPC, this discussion will be limited to processes relevant to the tool-ply friction during the forming process.

2.2.1 Manual and Automated Layup Process

The three major types of layup method used for FRPC are manual layup, automated tape laying (ATL) and automated fiber placement (AFP). The traditional, manual layup process involves manually laying down and shaping of cut prepreg in to a specific mold. A major constraint of this method is the low production volume and high labor cost associated with the process.^{3,17} Improvement in technology allows for faster production with automated lay-up processes such as the ATL and AFP methods.^{3 18} A schematic of the ATL is shown in Figure 4.

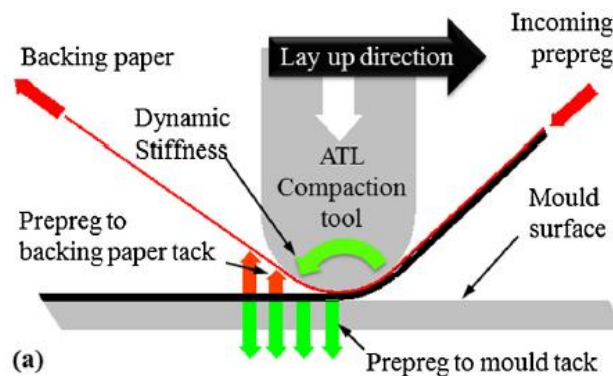


Figure 4. Simplified schematic of the ATL process¹⁹

In this process, the prepreg tape is held by a feed drum, and the material is guided across the flat or curved geometry at the specified feed temperature and velocity and compacted by the ATL

compaction tool head at the specified pressure.¹⁹ While this process has significant advantages in production volume and more consistent quality compared to the manual layup process, it requires rigorous computer simulation and design to ensure proper layup conditions.¹⁸ In general, sufficient tack is required to ensure that the prepreg is properly adhered to the mold surface and subsequent plies. Prepreg tack has shown to be dependent on the viscoelastic properties of the material at various processing parameters.¹⁹⁻²¹ The two main failure mechanisms observed in the ATL/AFP processes can be described as interfacial or cohesive failure shown in Figure 5.

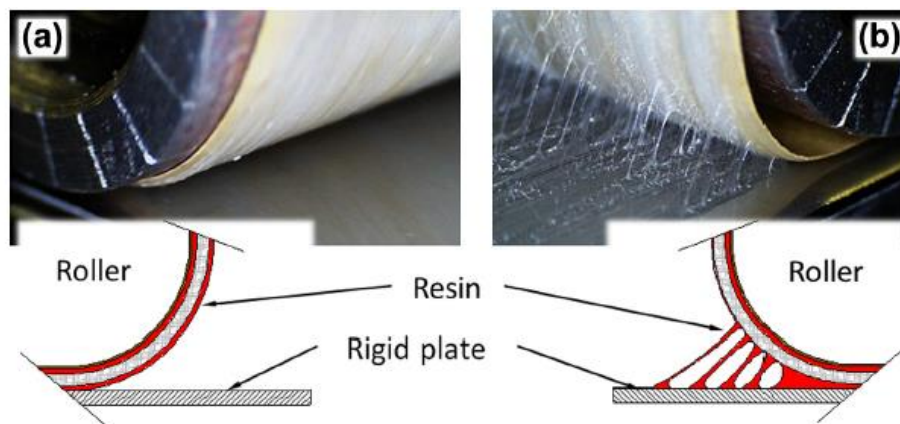


Figure 5. Interfacial (a) and cohesive (b) failure mode observed during peel-ply test¹⁹

The interfacial failure mode is characterized by insufficient resin deposition/bonding to the surface shown in Figure 5(a) whereas cohesive failure mode is characterized by excess resin deposition as seen in Figure 5(b). These failure mechanisms can result in delamination and improper resin distribution, which ultimately leads to a reduction in the quality of the final composite parts.^{18,19}

2.2.2 Compression Molding

One of the challenges in ATL and AFP is that these techniques are limited to forming laminates with flat or low to medium curvatures.¹⁹ FRPC with more complex shapes can be made by first lay-up of flat laminates with the automated lay-up process, followed by

compression molding to the desired geometry.¹⁰ The forming steps for compression molding of a FRPC laminate is shown in Figure 6.

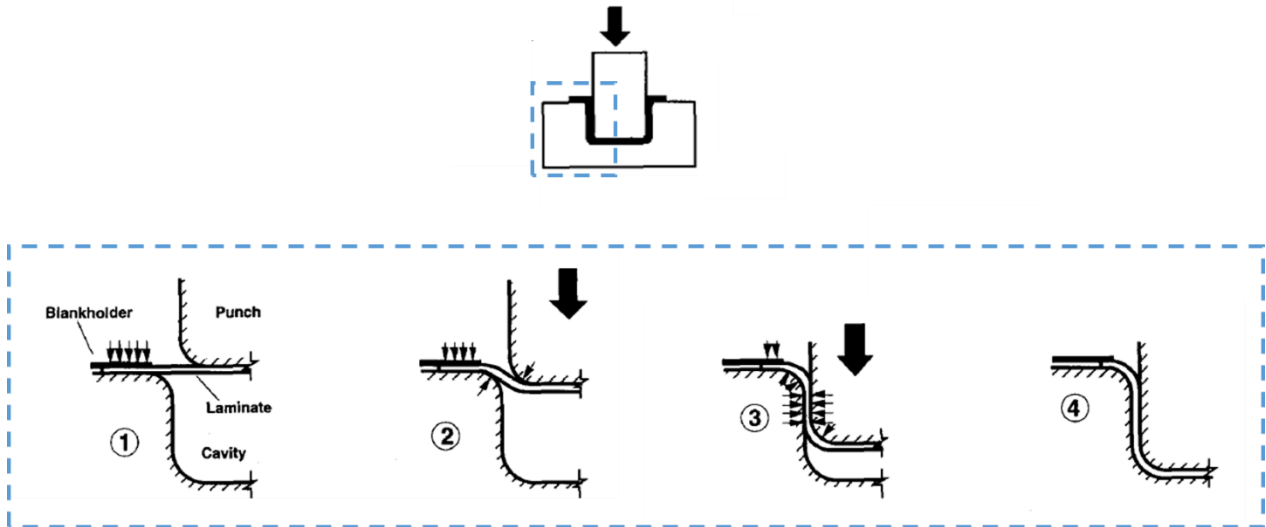


Figure 6. Overall (top) and detailed stages (bottom) of the compression molding process²²

During the first stage, the sample is heated to the desired temperature at a controlled heating rate. Once the mold and sample have reached the desired temperature, pressure is applied and the sample is quickly stamped (stages 2-3). The laminate is then held at constant pressure and temperature until the part is formed/cured (stage 4). It should be noted that wrinkles and surface defects can occur during the forming process due to friction at the contact point between the tool and laminate. These defects can result in reduction of final part properties due to residual stress formation in the cured laminates.^{10,22}

2.3 Tool-Ply Friction

One of the major challenges in the polymer composite forming process is the occurrence of wrinkling and shape distortion of the fabric caused by the surface differences between the forming tool and surface of the prepreg.⁸ In general, static friction is considered as friction between non-moving surfaces, and is dominated by adhesion between the contact surface

asperities, the time and mode of contact, whereas the kinetic friction is described by the friction between two moving surfaces and is dominated by the viscoelastic properties of the materials.⁵ The standard methods of determining the static and kinetic coefficient of friction of plastic films and sheeting can be found in ASTM D1894-14.²³ A schematic of the pull-out and pull-through method is shown in Figure 7.

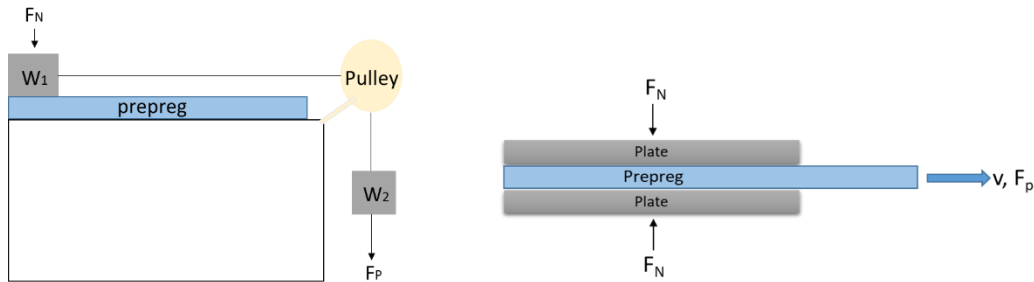


Figure 7. Schematic of pull-out (L) and pull-through (R) method

For the pull-out method, the sample is held under a weight and the weight is pulled over the top of the specimen, and the subsequent force and distance is recorded. The friction coefficient is then determined as the ratio of the pulling force over the normal force, where the static friction is the peak friction coefficient value, and the kinetic friction is the steady-state friction coefficient value over the sliding interval. For the pull-through method, the sample is sandwiched between two plates and pulled through at a controlled force at the desired temperature.²³

The effects of processing parameters on tool-ply friction of prepreg and epoxy systems have been studied extensively over the past few decades.¹⁸ The friction dependence of the surfaces in regards to processing parameters – such as forming temperature, pressure, and velocity – can be described by the Stribeck curve shown in Figure 8.

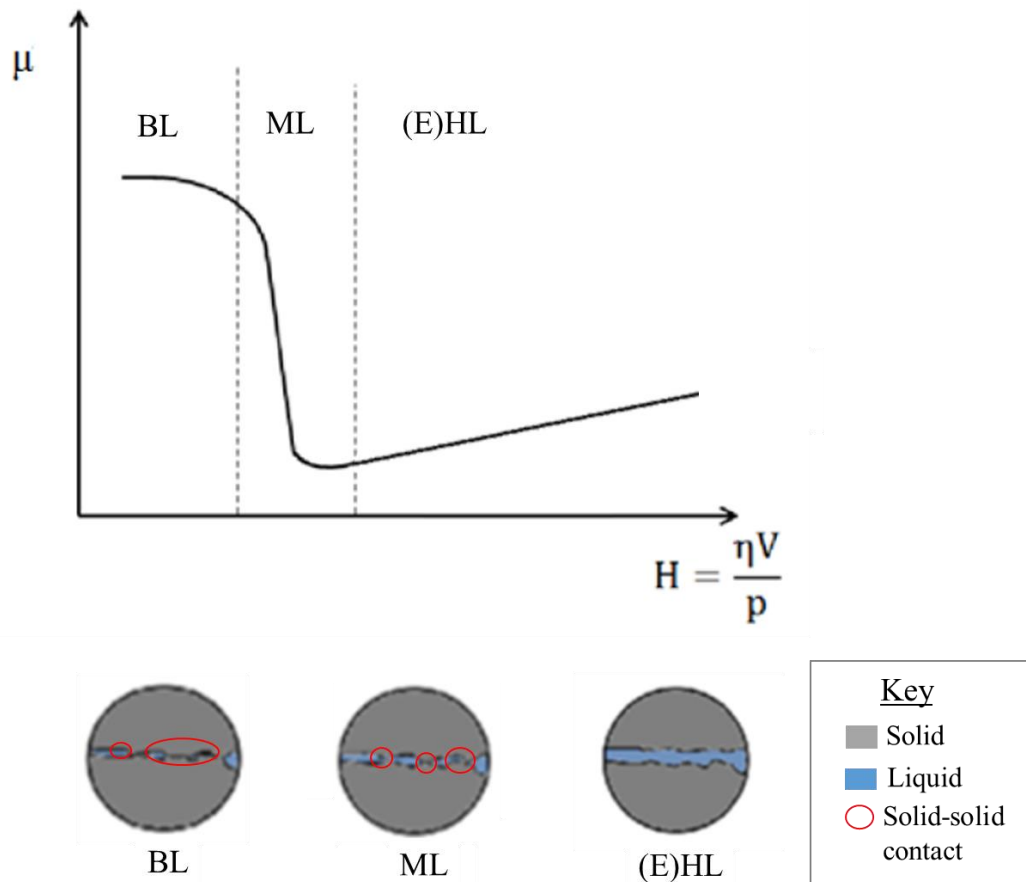


Figure 8. Generalized Stribeck curve with three regions. 1.) Boundary lubrication (BL) 2.) mixed lubrication (ML) and 3) elasto-hydrodynamic lubrication ((E)HL) ^{24,25}

Where μ is the friction coefficient, H is the Hersey number, η is the dynamic viscosity of the fluid, V describes the tooling velocity, and p is the pressure applied. The friction mechanisms are dependent on the contact and thickness of the fluid film between the surfaces. The first region is the boundary lubrication region (BL), also known as dry/Coulomb friction. This region is characterized by high friction values due to direct solid-solid contact between surfaces. The second region is a mixed lubrication region (ML), an overall reduction of friction is observed in this region as the surfaces are separated through a thin fluid film with some regions in contact. The third region is the elasto-hydrodynamic lubrication region (E)HL, where the surfaces are

completely separated by the fluid film.^{18,24,25} Fiber deformation and wrinkle formations are typically observed in the BL and ML regime due to tool-ply contact and high frictional forces.¹⁸

2.3.1 Effects of Testing Conditions on Tool-ply friction

In general, it has been shown that tool-ply friction increases with sliding velocity,²⁶ and decreases with increase in normal pressure and forming temperature.²⁵ This behavior is highly dependent on the material's bulk viscoelastic behavior, which is highly dependent on the forming time and temperature.^{22,26-30} Lower friction forces are typically observed with an increase in forming temperature, due to a decrease in resin viscosity.^{22,26,27} Increases in tool-ply friction at high forming temperatures have been reported in literature due to tool-fiber contact.^{22,26} For example, Lebrun et al.²⁶ examined the tool-ply friction of polypropylene/glass fabric and showed that samples exhibited Coulomb friction behavior above the melting temperature of the resin. Micrograph images of these samples showed fiber deformation perpendicular to the slipping direction. The author proposed that the friction behavior is dependent on both the resin viscosity and contact mechanism at various temperatures. At low temperatures, large friction forces were observed due to the high resin viscosity and viscous resistance of the system. A reduction in friction forces was observed at intermediate temperatures due to reduction in resin viscosity. However, at higher temperatures, the resin viscosity was sufficiently reduced. This lead to direct tool-fiber contact and fiber deformation that results in the increase in friction forces observed.²⁶ In addition, the authors found high friction values at high forming pressures and intermediate temperatures due to a combination of fiber deformation and viscous resistance of the resin, showing that friction behavior is dependent on the combination of processing parameters.^{26,28} Similar results were found by Twigg et al.²⁹ and Ersoy et al.³⁰ in their study of friction behavior of carbon fiber-reinforced prepreg as a function of temperature and cure. While an increase in

friction was observed with increase in forming temperature due to fiber-tool contact, a sharp increase was observed in both cases at the gelation point of the samples.^{29,30}

2.3.2 Effects of Fiber and Resin on Tool-Ply Friction

The frictional behavior has been shown to be dependent on fiber-weave, resin formulation, and mold geometry, as well.^{27,31-34} For example, Fetfatsidis et al.³², examined the tool-ply friction of Twintex ® twill-weave and plain-weave fabric with a pull-through method, and found that coefficient friction plain-weave is lower than twill-weave fabric due to the tighter weave pattern of plain-weave fabric. Similar results were found by J. Gorczyca et al.²⁷, where they compared the effect of fiber orientation on tool-ply friction. Lower friction and minimal surface distortion were observed for the plain-wave fabric as compared to the unidirectional fabric. In general, tighter weaves offer higher resistance against tool-ply movement, thus resulting in lowered friction and distortions.^{27,32} In addition to material type, the extent of deformation is also dependent on tooling geometry.^{27,31} Haanappel et al.³¹ examined friction behavior of unidirectional PEEK and satin weaved PPS glass prepreg with pull-through method. While both materials exhibited hydrodynamic friction behavior at various processing conditions with similar frictional values, larger deformations and wrinkle formations were observed in curved regions as compared to flat regions of the formed unidirectional PEEK material, due to less resistance against intra-ply shear during forming process.

Other material characteristics such as resin formulation and surface roughness have been found to effect the friction of prepreg systems.^{33,34} For example, Brostow et al.³³ showed that addition of 10 wt. % fluorinated poly(aryl ether ketone) (12F-PEK) to a commercial epoxy resin resulted in an overall 30% reduction in both dynamic and static friction of the cured sample. However, an increase in friction was observed for sample at a higher cure temperature compared

to samples cured at lower temperatures due to differences in surface roughness and contact area. The author reports phase separation of 12F-PEK at various conditions, which resulted in the surface migration of 12F-PEK to the surface, creating samples with rough surface characteristics. At the higher cure temperature, the rapid cure process effectively reduced the effects of phase separation and surface migration of the 12F-PEK particles, which produced samples with smoother surfaces but a higher contact area with higher frictional values.³³ The effects of processing parameters on surface roughness and interply-friction of two different types of unidirectional carbon fiber prepreg with a pull-through method was examined by Sun et al.³⁴ The author found that the sample with the rough surfaces had higher frictional values and exhibited Columbic-type friction, whereas the sample with the smooth surface had lower frictional values and exhibited hydrodynamic friction. This is due to the sample with the rough surface containing asperities with contact areas greater than the contact areas of the lubricating film, resulting in contact of the asperities between the piles. The sample with the smooth surface had lower frictional values because the surface roughness was less than that of the lubricating film. This allowed for the surfaces to be fully separated by a lubricating layer.³⁴

Considerable efforts have been put forth to develop models to describe tool-ply friction with respect the processing parameters, material quality/type, and forming geometry.^{5,25,35} A challenge with traditional pull-out and pull-through methods is that they are often time-intensive and results are limited to the specific equipment. While the methods mentioned above include the effects of temperature, time, and pull out speed, variations in material structure – such as the change in resin viscosity and cure as a function of temperature and time – have to be determined by various other equipment and methods, such as rheology and differential scanning calorimetry (DSC).⁵

2.3.3 Rheological Characterization of Tool-Ply Friction

An alternative method of studying prepreg friction has been developed using a commercial rheometer to examine the relationship between the tool-ply friction and the viscoelastic properties function of processing parameters.^{4,5,24,25,35} Specifically, the application of principles of friction, lubrication, wear, and the relative interaction of surfaces in motion can be described as a combination of tribology and rheology.³⁵ Frictional measurements of composites can vary widely due to the measurement technique or test instruments used. For example, Harrison et al.⁵ studied the tool-ply friction of Twintex® glass-polypropylene sheets at various temperatures, pressures, and sliding velocities using pull-through and pull-out methods and compared the results measured on a commercial rheometer. While Stribeck analysis of the material at various conditions and measurement methods showed that the material exhibited (E)HL friction behavior, they had difficulties in comparing the exact parameters, as the normal force and velocity that can be achieved by a commercial rheometer is much lower than the pull-through and pull-out method.⁵ Kavenhpour et al.³⁵ utilized a commercial rheometer with a modified ring geometry to effectively increase the pressure limitation of the instrument, and studied the effects of processing parameters on friction behavior and surface roughness of various polymer materials. The author developed a dimensionless gap-shift factor to account for the variation in surface roughness as a function the gap height of the fixture at various processing parameters.³⁵ Vu, I.²⁴ utilized the modified annulus geometry to examine the tool-ply friction of composite prepreps and dry textile fabrics with a rheometer at various processing conditions. The author concluded that frictional mechanisms of the prepreg material display a combination of both columbic and hydrodynamic friction, which is consistent with behavior seen in the mixed lubrication regime of the Stribeck curve.²⁴ Thije et al.²⁵ utilized a similar approach developed by

The transformation of material state as a function degree of cure (α) at various time and cure temperatures can be described by three critical events- gelation, vitrification, and cure. During the initial stages of processing, the prepreg is a B-stage resin that exhibits characteristics of un-gelled glass. As the material is heated to the glass transition temperature, the material transforms from un-gelled glass to viscous liquid. At gelation, the material transforms from a viscous liquid into a rubbery-gel state. The gel point is one of the most critical transition points in regards to processing, as it describes point at which the material loses the ability to flow and be processed due to the onset of irreversible 3-D network-formation of the system.³⁶⁻³⁸ Vitrification is the transition from rubbery-gel to a glassy-gel state, which can occur during the cure process depending on the forming temperature and heating rate. At this state, the cure kinetics of the resin become diffusion controlled, which results in an overall reduction in the rate of reaction of the cure process. The system will reach a critical crosslinking-density prior to complete conversion, resulting in a system with a lower glass-transition temperature and degree of cure. Variations in processing parameters during the cure cycle (such as increasing the cure temperature to above the final glass transition temperature) is generally required overcome vitrification to achieve maximum cure.³⁸⁻⁴¹ It should be noted that the heating rate should be carefully controlled to prevent excess resin flow prior to gelation.^{38,42}

The viscoelastic behavior of thermosetting systems has been studied extensively in literature. Rheological analyses are often coupled with kinetic modeling determined through DSC measurements to model the viscosity dependence of thermosetting systems as a function of time and cure.⁴²⁻⁴⁴ Early works on predicting the cure behavior of prepreg systems were based on the chemorheology of the neat epoxy systems. In particular, Macosko et al.³⁹ developed a model in 1985 to determine the optimal processing conditions for thermosetting resins by combining

polymerization kinetics, branching theory and rheological measurements. Common issues observed in their rheological model were caused by vitrification and phase separation. Dynamic viscosity data of their epoxy sample showed that increasing the temperature during the cure cycle can overcome vitrification and restart the cure reaction.³⁹

In addition to determining the optimal flow and processing conditions, the study of TTT and chemorheology has been used to examine the effects of sample quality as the viscoelastic properties of prepreg materials can change dramatically depending on environmental conditions such as temperature, moisture content, and resin staging.^{45,46} For example, Miller et. al.⁴⁶ examined effects of prepreg out-time on the viscoelastic properties on the materials using DMA, DSC, rheological and tack measurements. They found an overall reduction in t_{gel} and t_{vit} in the aged sample compared to the fresh sample. Similar results were found by Apicella et al.⁴⁵, where physical properties and durability of the final product were worse in the aged sample as compared to the unaged sample.⁴⁵

CHAPTER 3

MATERIALS AND METHODS

3.1 Materials

The material studied in this work was HexPly® unidirectional (UD) prepreg (M77/38%/UD300/SGL-50K), supplied by Hexcel, Duxford, UK. The material used is a 50K high strength carbon fiber tow, with a fiber areal density of 300 gsm, pre-impregnated with M77 epoxy resin (38% resin content). The M77 resin used is a low tack, fast-curing epoxy with a cure time of two minutes at 150°C with a long shelf life of 18 months at -18°C, and 6 weeks at room temperature. The cure cycle of the resin is between 80°C-160°C, with a cure time of 480mins-1.5mins at various temperatures shown in Table 1.⁴⁷ The M77 resin is specifically designed for compression molding process with complex geometries. The material is suited for high volume production processes such as the manufacture of automotive parts and consumer products, such as skis.⁴⁷

Table 1. Cure cycle of HexPly® M77 epoxy resin (obtained from HexPly datasheet)⁴⁷

Temperature [°C]	Time [min]
80	480
90	90
100	40
110	18
120	7
130	5
140	3
150	2
160	1.5

3.2 Equipment

3.2.1 Torsional Rheometer

In this study, the commercial torsional rheometer (Anton Parr MCR 302 fitted with a CTD 450 convection temperature chamber) shown in Figure 10. was used to measure the tool-ply friction, viscoelastic properties and time/temperature dependent cure of the sample.



Figure 10. Anton Parr MCR 302 Rheometer with CTD 450 convection temperature chamber

Torsional rheometers are commonly used to measure viscosity and viscoelastic properties of samples in relatively low shear rate ranges, typically from $0.001 - 100 \text{ s}^{-1}$. The two primary modes of testing in a rotational rheometer are steady shear and small-amplitude oscillatory shear (SAOS). Steady shear mode is typically used to determine the bulk shear viscosity (η) and/or time dependent η of a sample, while SAOS is particularly useful in measuring the viscoelastic properties such as the complex viscosity (η^*), shear storage modulus (G') and shear loss modulus (G''), of the sample.⁶

A CTD 450 convection temperature chamber is fitted to the rheometer for precise temperature control of the system. The heating system has a temperature range of -150-450°C, with a maximum heating rate of 50°C/min, and cooling rate of 35°C·min⁻¹.⁴⁸ The relevant technical specifications of the MCR 302 with the CTD 450 chamber are shown in Table 2.

Table 2. Process limitations of Anton Parr MCR 302 rheometer fitted with CRD 450 heating chamber

	Temperature [°C]	Normal Force [N]	Torque [N·m]	Angular velocity [rad·s ⁻¹]
Minimum	-150	0.005	5·10 ⁻¹⁰	1·10 ⁻⁹
Maximum	450	50	0.2	314

The instrument is fitted with a stationary bottom plate and a rotating upper plate that operates under the specified inputs. Parallel plate fixtures are commonly used for oscillatory measurements in the linear-viscoelastic region. One of the benefits of using the parallel plate geometry is the ability to monitor gap height as a function of experimental conditions.⁴⁹ However, it should be noted that the shear rate is non-uniform across the plate. With regards to friction measurements, parallel plate fixtures are often used in literature with a modified annulus geometry to minimize shear rate variations across the geometry, and to increase the effective contact pressure to values similar to forming processes.^{4,5,24,35} The plates used in this study were 6061-T6 aluminum plates. Parallel plates with 25 mm diameter were used for the bottom plates, while the top plates used in this study were either 25mm parallel plates or modified annulus geometry (1mm ring, shown in Figure 11). The pressure limitations of the plates and rings used in this study are shown in Table 3.

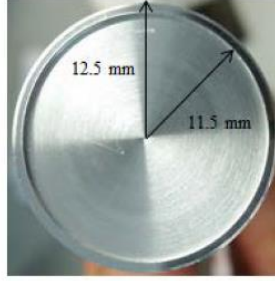


Figure 11. Modified plate geometry with 1mm annulus²⁴

Table 3. Contact pressure range of plate versus modified annulus geometry

	Contact Area [m ²]	Minimum Pressure [Pa]	Maximum Pressure [Pa]
Parallel Plate (12.5mm)	$4.91 \cdot 10^{-4}$	10	$1.0 \cdot 10^5$
Modified Ring (1.0mm)	$7.54 \cdot 10^{-5}$	66	$6.6 \cdot 10^5$

3.2.2 Imaging

Magnified surfaces images of sample were taken with a digital C-mount camera (GXCAN-5) with a 4x objective.

3.3 Methodology

3.3.1 Sample Preparation

Unidirectional carbon fiber prepreg supplied by HEXCEL (HexPly® M77/38%/UD300/50K), were kept in a sealed bag and stored in a freezer between tests to prevent cure advancement of the B-staged prepreg. The prepreg was moved to room temperature at 22°C and was cut into 28 mm x 28 mm squares. Sample size and shape were kept consistent to minimize variation in measurements due to edge effects.

Samples were loaded with the fiber orientation parallel to the machine (Figure 12) and adhered to the bottom fixture with cyanoacrylate (MXBON®). For the cure experiments, a new set of plates was used for each test. Plates were re-used for experiments conducted below 80°C.⁴⁷ The top and bottom geometry were thoroughly cleaned with acetone between tests to remove

residual resin transferred from previous experiments.²⁴ A brief study on sample adhesion type and shape on rheological properties can be found in Appendix A.

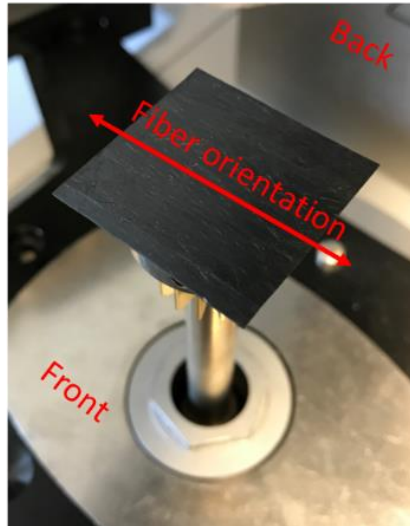


Figure 12. Prepreg fiber orientation in rheometer

3.3.2 Sample Heating

For experiments conducted above room temperature, the prepreg was heated from 20° to the specified temperature at a specified heating rate. A 5-minute dwell time was implemented after the ramp cycle due to eliminate thermal lag effects.

3.3.3 Viscoelastic and Cure Analysis

3.3.3.1 Determining the Linear Viscoelastic Region

Before running any tests, it is important to determine the linear viscoelastic region (LVE) of the sample to evaluate the relationship between molecular structure and viscoelastic properties. At constant G' (within the LVE region), the sample structure remains unchanged. Strain rates above the LVE region indicates structure instability (i.e. structure break down). Test parameters included oscillatory strain sweep (0.1% to 100%) with a constant frequency of 1 Hz at ambient temperature and a normal force of 5N. To determine the LVE region, G' (Pa) and G'' (Pa) was plotted against % strain. The LVE region is the region of strain where G' remains

constant, and below the critical strain at the onset of non-linear G' behavior.^{50,51} The determination of LVE can be found in Appendix A.

3.3.3.2 Viscoelastic Measurements

The viscoelastic and structural properties were characterized with oscillatory frequency sweep tests at strains below the critical strain of 0.07% found from the LVE test. Plots of G' , G'' vs. time/temperature or $\tan \delta$ (G''/G') vs time/temperature can be made to examine the viscoelastic properties of the material. If G' is greater than G'' or if $\tan \delta < 1$, the sample predominantly behaves as a solid, and if G'' is greater than G' or if $\tan \delta > 1$, the sample behaves predominantly as a viscous fluid.^{40,50,51}

3.3.3.3 Effects of Heating Rate on Minimum Viscosity

With regards to thermoset laminate processing, sufficient wetting and flow are required during the molding process to ensure proper forming of the laminate system. The ideal forming range of the material can be determined by locating the time and temperature required to reach the minimum viscosity value.⁴² At the minimum viscosity, the resin would have minimal flow resistance. Therefore, pressure should be applied at or near this time and temperature interval to maximize resin distribution. It should be noted that the processing window varies depending on the heating rate.⁴² The effects of heating rate on the minimum viscosity of the prepreg system were examined under dynamic oscillatory (SAOS) mode at 0.01 strain %, normal force of 5N, and a heating rate of 1, 2, 4, 5°C/min from 20-140°C with a parallel plate geometry. The normal force of 5N was chosen based on the maximum normal force used for the tool-ply friction experiments.

3.3.3.4 Effects of Temperature on Resin Staging

The effects of cure temperature on the cure behavior of the prepreg system was conducted under dynamic oscillatory (SAOS) mode at 0.05 strain %, normal force 5N, cure temperature of 90°C, 100°C, and 110°C and cure time of 120, 55, 24 minutes (respectively) at a heating rate of 10°C·min⁻¹. The resin staging procedure is similar to the method listed by Corbridge et al.⁵²

The degree of conversion is typically found by examining the cure kinetics determined with DSC measurements.^{40,53,54} In this study, the degree of conversion (α) was determined based on the shear viscoelastic properties of the material by using Equation 1.^{40,44}

$$\alpha = \frac{G'(t) - G'_0}{G'_\infty - G'_0} \quad (1)$$

where α is the degree of conversion, $G'(t)$ is the storage modulus measured at the specific time point, G'_0 is the minimum storage modulus over the whole interval, and G'_∞ is the maximum storage modulus in the cured interval.^{40,44}

3.3.3.5 Time Temperature Transformation (TTT) Study

The relationship between the viscoelastic properties and cure was examined with a TTT study. The processing window for the lay-up and molding process was examined by determining the sub-ambient glass transition temperature ($T_{g,sub}$), gel point (t_{gel}), vitrification point (t_{vit}), and cure point (t_{cure}) as a function of cure.^{37,43,55-57} These values were obtained from analyzing the experimental data obtained from resin staging experiments with techniques described below.

The $T_{g,sub}$ is synonymous to the glass transition temperature of a polymer, where it is the transition of an uncured prepreg system from a glassy to rubbery state. The $T_{g,sub}$ is generally a range of values that is dependent on material quality, formulation and age. It can be quantified as

the maximum of the G'' value on a G'' versus time plot, or determined at the maximum $\tan \delta$ on a $\tan \delta$ versus time plot.⁵⁶

The gel point describes the onset of irreversible 3-D network formation of the system. There are various methods to determine t_{gel} at the isothermal cure conditions, including: (1) the crossover point of G' and G'' (or when $\tan \delta = 1$); (2) the point at which viscosity approaches infinity; (3) the point at which $\tan \delta$ drops suddenly; and (4) the point at which $\tan \delta$ is independent of frequency.^{43,55,57,58} It is important to note that the crossover point listed in condition (1) was based on the assumption that the crossover is independent of the frequency measured in the SAOS experiments.⁵⁸ The critical gelation time can be determined by Equation 2.^{37,55}

$$t_{gel} = A \exp\left(-\frac{E}{RT}\right) \quad (2)$$

where t_{gel} is the time required to reach gelation at the isothermal condition, A is the pre-exponential factor, E is the apparent activation energy in $\text{kJ}\cdot\text{mol}^{-1}$, R is the universal gas constant in $(\text{kJ}\cdot\text{mol}^{-1}\cdot\text{K}^{-1})$, and T is the isothermal curing temperature in (K).^{37,55} These values can be determined by linearizing the above equation and plotting $\ln(t_{gel})$ versus $1/T$.

The time it takes for the sample to transform from a rubbery gel to solid to a glassy gel can be described as t_{vit} . This point can be determined at the max G'' on a G'' versus time plot.^{37,55} The t_{cure} is the point at which the degree of conversion reaches maximum cure. This can be found as the time in which maximum α is reached on a conversion (α) versus time plot.^{37,55}

3.3.4 Tool-ply Friction Measurements

The effects of processing conditions on the frictional sliding behavior of prepreg material were conducted with the parallel plate ring geometry at parameters listed in Table 4. The tests were conducted at the specified temperature and normal force until a sliding distance of 100

mrad (or 5.73°) is achieved. A brief study on the effects of surface roughness on frictional sliding tests can be found in Appendix B. The tool-ply friction measurements were based on the method developed by Kavenpour et al., and Vu, I.^{24,35}

Table 4. Test parameters for frictional sliding tests below 80°C

Temperature [$^\circ\text{C}$]	20	40	60	
Sliding velocity [mrad/s]	1	10	15	100
Normal Force [N]	0.5	2	5	

The frictional sliding test parameters as a function of resin staging were examined with the parallel plate geometry at 90°C , $10 \text{ mrad}\cdot\text{s}^{-1}$, and a normal force of 5N. The degree of conversion (α) of the samples was calculated with spline fitting (in MATLAB) the time at each sliding interval with the prepreg cure time measured from the resin staging experiments.

3.3.4.1 Friction Calculations

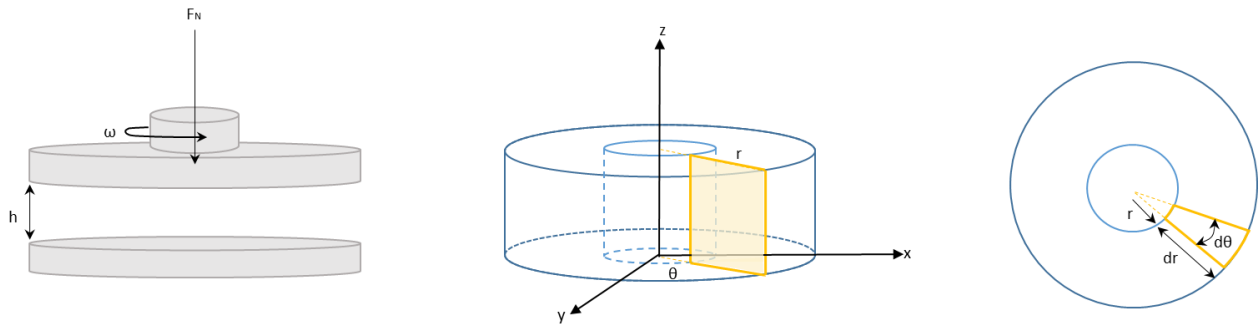


Figure 13. Schematic diagram of parallel plate rheometer plates (left), wedged sample in cylindrical coordinates (middle), and elemental area of a specimen (right)

The friction force based on the Amontons's law is described by Equation 3, where μ is the coefficient of friction, F_f is the frictional force in N, and F_N is the normal load applied on the object.^{24,59}

$$F_f = \mu F_N \quad (3)$$

The normal load applied on the object over a certain area is described by Equation 4 below, where P is the applied pressure, and A is the area of the sample.

$$F_N = PA \quad (4)$$

The area of the annulus can be determined by integrating Equation 5 from $\theta = 0$ to $\theta = 2\pi$ and from $r = R_1$ to $r = R_2$, where R_1 is the inner radius and R_2 is the outer radius shown in Equation 6.

$$dA = r dr d\theta = \int_0^{2\pi} \int_{R_1}^{R_2} r^2 dr d\theta \quad (5)$$

$$A = \pi(R_2^2 - R_1^2) \quad (6)$$

Assuming a uniform pressure over the contact area, the pressure for the annulus is determined by substituting Equation 6 into Equation 4.

$$P = \frac{F_N}{A} = \frac{F_N}{\pi(R_2^2 - R_1^2)} \quad (7)$$

The torque (M) required for slip can be described by Equation 8.

$$M = F_f r \quad (8)$$

The torque required for slip for the annulus can be determined by integrating the above equation (assuming an uniform contact pressure and coefficient of friction over the elemental area) and is shown in Equation 9.

$$M = \mu P \int_0^{2\pi} \int_{R_1}^{R_2} r^2 dr d\theta = \frac{2\pi}{3} \mu P (R_2^3 - R_1^3) \quad (9)$$

By substituting Equation 7 and Equation 3 into Equation 9, the torque required for slip for an annulus is shown in Equation 10.

$$M = \frac{2F_f(R_2^3 - R_1^3)}{3(R_2^2 - R_1^2)} \quad (10)$$

The frictional force is represented in Equation 11.

$$F_f = M \frac{3(R_2^2 - R_1^2)}{2(R_2^3 - R_1^3)} \quad (11)$$

The coefficient of friction is represented in Equation 12.

$$\mu = \frac{M}{F_N} \frac{3(R_2^2 - R_1^2)}{2(R_2^3 - R_1^3)} \quad (12)$$

The static and kinetic friction values were determined by plotting the F_f or μ against the deflection angle as shown in Figure 14. Where F_s and μ_s were determined at a single maximum point, and the F_k and μ_k are an average over the steady state interval.

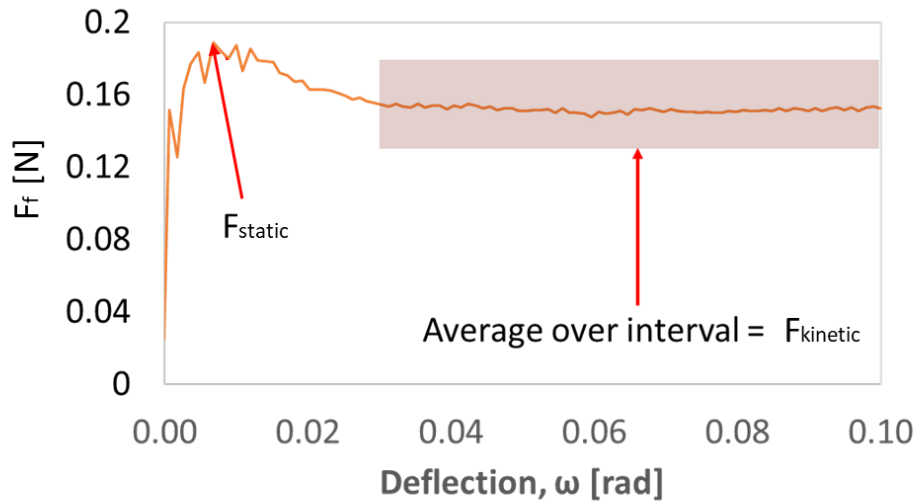


Figure 14 . Sample friction plot used to determine F_s and F_k

CHAPTER 4

EXPERIMENTAL RESULTS AND DISCUSSION

4.1 Rheological Analysis of Viscoelastic and Cure Behavior

The objective of this section is to determine the relevant processing window for the lay-up and molding process of HexPly® M77/38%/UD300/50K prepreg. The effects of processing parameters such as heating rate and temperature on the viscoelastic properties and cure characteristics will be explored in the following sections. The general viscoelastic behavior at various processing conditions will be used to predict tool-ply friction mechanisms of the system. Materials formed outside of the optimal processing range can result in fiber distortions. For example, materials formed below the glass transition temperature can exhibit brittle failure due to high viscosity and high friction present between the tool-ply interface.^{18,19} An understanding of the relationship between the viscoelastic properties and tool-ply friction can be used to optimize the forming process. As mentioned previously, the combination of the resin and fiber introduces complexities over the cure interval due to differences in epoxy formulation, fiber content, sample aging, and measurement conditions.^{4,45,46} As such, it is important to characterize the viscoelastic properties in the composite processing / forming regions, including minimum viscosity and gelation point.

4.1.1 General Viscoelastic Behavior

The cure characteristics can be determined by identifying the viscoelastic properties such as G' , G'' and $\tan \delta$ over the cure interval. If G' is greater than G'' or if $\tan \delta < 1$, the sample will predominantly behave as an elastic solid, and if G'' is greater than G' or if $\tan \delta > 1$, the sample behave predominantly as a viscous fluid.^{50,51} A typical cure diagram of a prepreg sample

conducted under SAOS mode at 0.01 strain %, 1Hz, normal force of 5N, and a heating rate of 10°C/min from 20-140°C with a parallel plate geometry is shown in Figure 15.

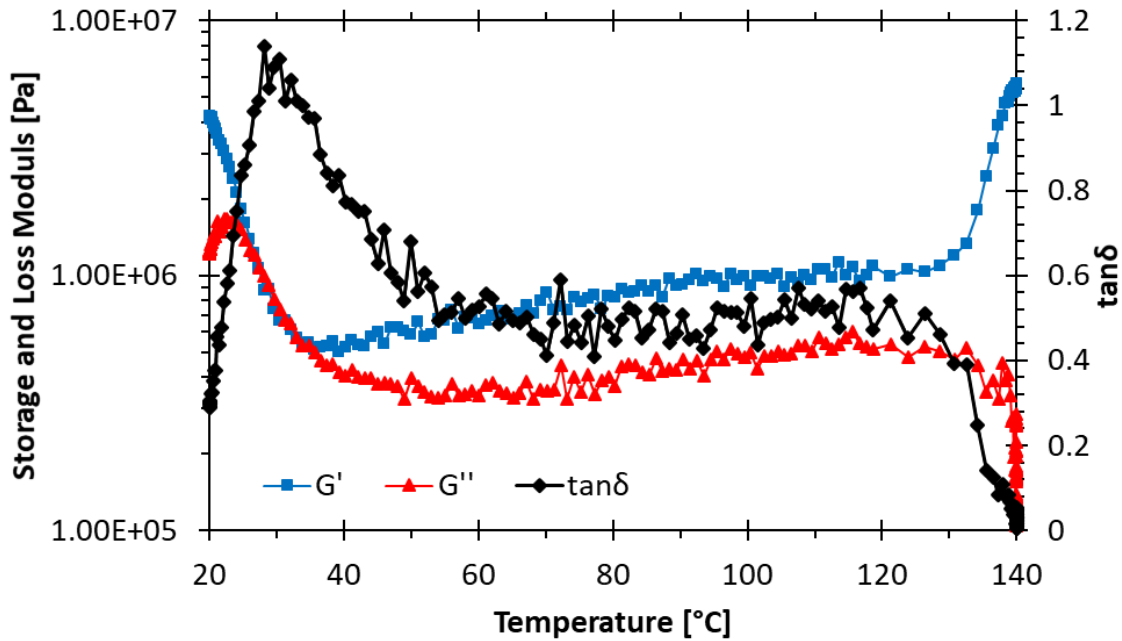


Figure 15. Typical cure diagram of viscoelastic behaviors obtained through rheology

A large G' and low $\tan \delta$ of 0.28 was observed at the onset of the experiment, suggesting that at low temperatures, the material behaves as a glassy solid. As the sample was heated from 20°-30°C, a decrease in G' and increase in G'' was observed, which is indicative of the glass transition temperature region due to the increase in molecular mobility at higher temperatures.

As the temperature continue to increase from 30°C-120°C, the G'' plateaus as typically observed for a rubbery plateau region. This is due to the fact that the matrix is partially cured in its B-stage form, which inhibits molecular mobility compared to an uncured system (such as an A-stage epoxy resin). A sharp increase in G' was observed at around 126°C, which is indicative of the formation of 3-D network system. While the onset of gelation of a thermosetting polymer is typically determined at the G' and G'' crossover point, this behavior was not observed in the present system. The lack of G' and G'' crossover point during gelation of prepreg has been

reported in literature due to the presence of the carbon fiber.^{60,61} This is because the neat resin system primarily exhibits viscous liquid-like behavior, while the carbon fiber exhibits elastic solid-like behavior.^{60,62} Since the present system is a high-fiber content prepreg (62% volume fiber), the system should exhibit fiber dominated properties, which contributes to the effective increase of G' observed in the system. It should be noted that while SAOS tests were conducted below the LVE region of the material (shown in Appendix A), the LVE of the material should be examined at a wider set of temperatures to verify that the material is within the LVE region at higher temperatures.

4.1.2 Effects of Heating Rate on Minimum Viscosity

With regards to thermosetting laminate processing, sufficient wetting and flow is required during the molding process to ensure proper resin distribution between the fibers and laminate plies. The forming range of the prepreg can be determined by locating the time ($t_{\eta^*_{\min}}$) and temperature ($T_{\eta^*_{\min}}$) at the minimum viscosity (η^*_{\min}) point over the heating interval. Pressure should be applied at or near the minimum viscosity to ensure minimal resin resistance and maximum flow.⁴² It should be noted that the processing window at which pressure should be applied is dependent on the heating rate, as a higher heating rate generally results in a lower minimum viscosity point and a shorter consolidation time.⁴

The effect of heating rate on minimum viscosity of the prepreg system was conducted under SAOS mode at 0.01 strain %, normal force of 5N, and a heating rate of 1, 2, 5, 10°C/min from 20-140°C with a parallel plate geometry. Changes in the viscosity profile over the measurement interval as a function of heating rate is shown in Figure 16, with the corresponding parameters at the minimum viscosity point listed in Table 5.

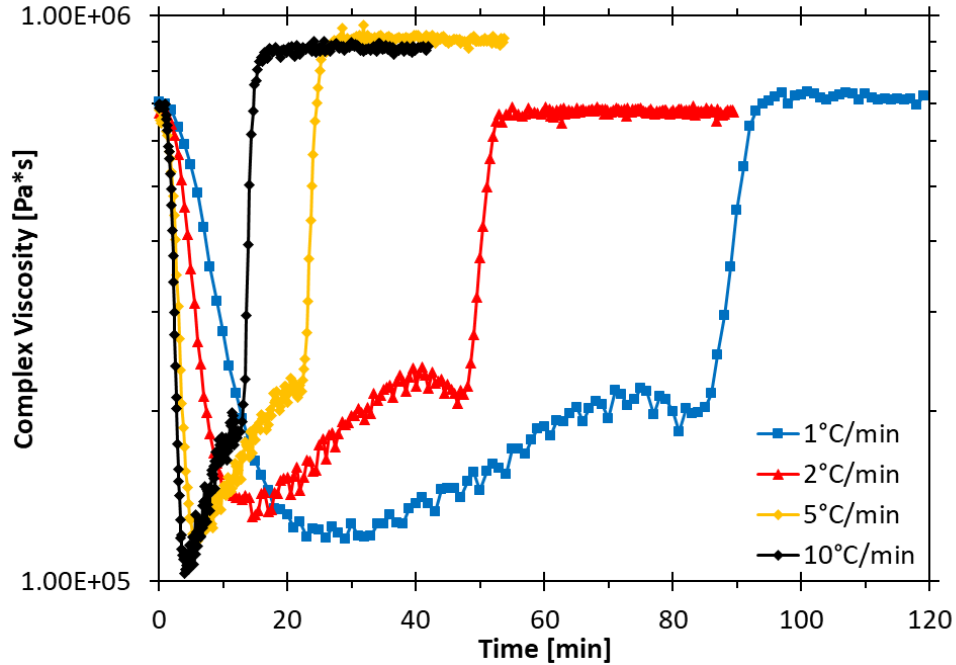


Figure 16. Evolution of complex viscosity over time at various heating rates

Table 5. Corresponding processing parameters at the minimum viscosity point for various heating rates

Heating Rate [°C·min ⁻¹]	η^*_{\min} [Pa·s]	$T_{\eta^*_{\min}}$ [°C]	$t_{\eta^*_{\min}}$ [min]
1	$1.19 \cdot 10^5$	48	29
2	$1.30 \cdot 10^5$	45	15
5	$1.18 \cdot 10^5$	40	6
10	$1.03 \cdot 10^5$	39	4

During the heating interval, a reduction in viscosity was observed until the minimum viscosity point due to the increase in molecular mobility at higher temperatures. As the heating rate increased from $1^\circ\text{C}\cdot\text{min}^{-1}$ to $10^\circ\text{C}\cdot\text{min}^{-1}$, an overall decrease in η^*_{\min} was observed from $1.19 \cdot 10^5$ to $1.03 \cdot 10^5$ Pa·s, with a decrease in $T_{\eta^*_{\min}}$ from 48 to 39°C, and a decrease in $t_{\eta^*_{\min}}$ from 29 to 4 minutes. Beyond the minimum viscosity point, the complex viscosity increased due to network formation, resulting in a reduction in molecular mobility of the system. This is followed by a slight decrease in the complex viscosity, and a sharp increase and plateau in the complex viscosity, which signifies the gelation and cure of the sample. The increase in heating rate

reduced the time between the minimum viscosity point to gelation (approximately 10 minutes for $1^{\circ}\text{C}\cdot\text{min}^{-1}$ and less than 1 minute for $10^{\circ}\text{C}\cdot\text{min}^{-1}$), which also reduced the time available for consolidation. The observed viscosity profile showed that a higher heating rate corresponds to a lower η^*_{min} , $T_{\eta^*_{\text{min}}}$, $t_{\eta^*_{\text{min}}}$, and an earlier onset of gelation. The point at which pressure should be applied for the forming process should be at or around the minimum viscosity point and adjusted depending on the heating rate.

The evolution of viscosity as a function of temperature of the neat epoxy system (obtained from Hexply® M77 product data sheet)⁴⁷ is compared to the prepreg sample in Figure 17.

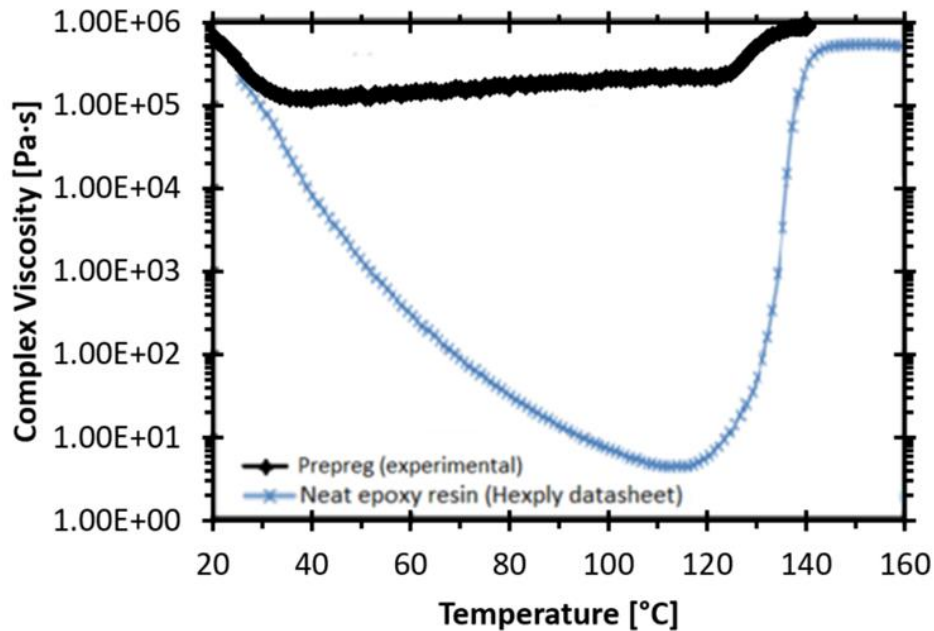


Figure 17. Viscosity profile of the neat epoxy resin system (Hexply® M77 product data sheet⁴⁷) compared to M77 prepreg (experimental) at a heating rate of $5^{\circ}\text{C}\cdot\text{min}^{-1}$

There are several significant differences between the viscosity profiles of the epoxy system as compared to the prepreg system. First, above approximately 30°C , the overall viscosity of the prepreg system was higher than the viscosity of the neat epoxy system as represented by the manufacturer. The higher viscosity values are consistent with samples that contain fibers. This is

due to the presence of the fiber in the prepreg resisting deformation, which contributed to the increase in the complex viscosity of the sample.⁶⁰ Second, the increase of the viscosity of the prepreg was observed at a much lower temperature (40°C) compared to the epoxy (118°C). The early onset of cure behavior is similar to samples with advanced resin staging.⁶³ The presence of B-stage resin contains partially cross-linked monomers compared to an uncured system, which would require less thermal energy to initiate the crosslinking reaction.

It is interesting to note that a second peak (with a much higher slope) was observed at 126°C in the prepreg. One possible explanation for this behavior is that the prepreg contains different types of epoxy, where the onset of network formation for one phase occurred at the lower temperature (40°C), and the network formation of the second phase occurred closer to the value of the neat epoxy at the higher temperature (126°C). However, deviations in prepreg viscosity have been reported in literature due to changes in resin distribution and prepreg compressibility at higher temperatures.^{24,41,63,64} This occurs because the rheometer maintains a constant normal force by adjusting the gap height. As resin viscosity decreases over the heating interval, the material softens, which results in an increase in resin distribution across the surface of the prepreg and an effective reduction in gap height that allows the tool to move closer to the fiber.²⁴ As such, the differences observed in the viscosity profile of prepreg system could be due to an artifact of the measurement technique caused by the changes in the resin distribution and contact mechanism between the tool-ply systems at higher temperatures.

To examine the effects of temperature in changes in gap height and viscosity over the measurement interval, dynamic oscillatory (SAOS) tests were conducted at 22°C, 40°C, and 60°C, 5N, 0.05% strain, and 1 Hz with a ring geometry with a measurement time of 60 minutes. The changes in gap height as a function of time and temperature are shown in Figure 18. It is

predicted that at higher temperatures, the reduced resin viscosity will allow for an increase in resin distribution across the surface of the prepreg system and an effective decrease in the gap height, as monitored by the rheometer. Minimal gap change would be expected at the lower temperature due to the high resin viscosity. In addition, an increase in the complex viscosity would be expected if there is direct tool-fiber contact between the systems.

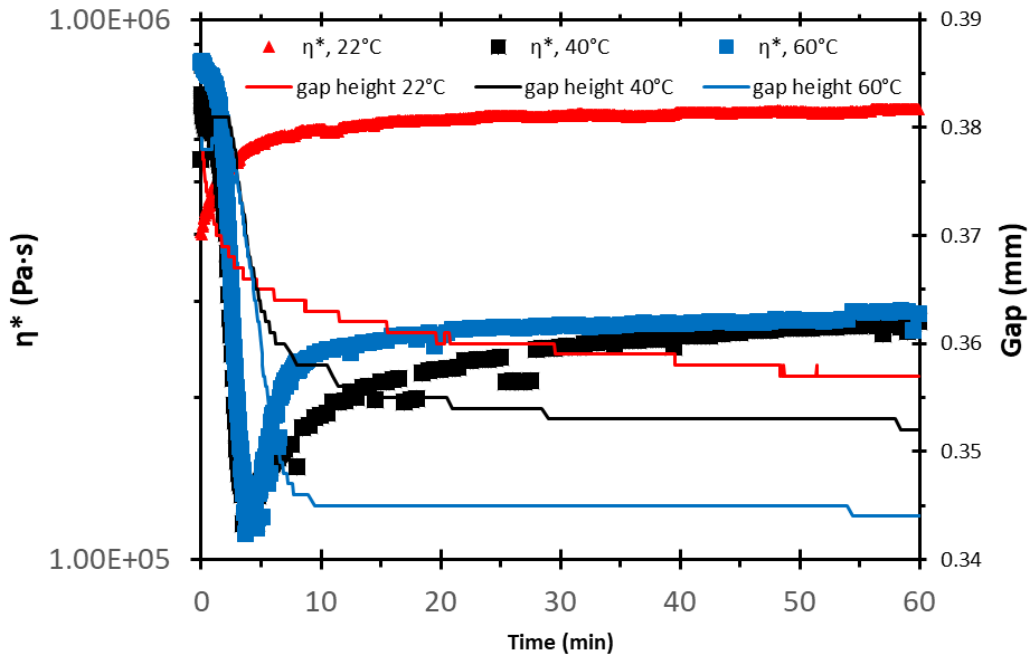


Figure 18. Changes in complex viscosity and gap height over the measurement interval

A large decrease in complex viscosity and gap height was observed during the heating interval for the 40°C and 60°C samples (0-7 minutes for 40°C sample, and 0-9 minutes for 60°C sample). This was followed by an increase and plateau of the gap height and complex viscosity over the measurement interval. This supports the prior hypothesis, where the reduction of resin viscosity at higher temperatures allows for an increase in resin mobility and distribution across the surface of the prepreg, which enables the tool to move closer to the fiber. The increase and plateau of the complex viscosity at the lower gap height could be due to direct tool-fiber contact at the lower gap height, followed by localized compaction of the prepreg.⁶⁴ It is interesting to note that

changes in gap height were also present in the 22°C sample. While this behavior was not expected due to the high viscosity of the sample measured at 22°C, this suggests that localized deformation can still occur between the tool-ply surface, depending on the applied pressure between the contacting regions.⁶⁴ While the changes in gap height can be reduced by decreasing the normal force value, the higher normal force applied in this study was more representative of the forming conditions.

The relative resin distribution and fiber deformation of the system can be further examined by comparing viscoelastic properties at the critical gap height region (onset of increase in complex viscosity) shown in Table 6, and the steady-state gap height region (plateau of complex viscosity) shown in Table 7.

Table 6. Onset of increase in complex viscosity at various temperatures (“critical gap height region”)

Sample [°C]	Time [min]	Temp [°C]	Viscosity [Pa·s]	G' [Pa]	G'' [Pa]	tan δ [-]	gap change [mm]
22	0.05	22.4	$3.99 \cdot 10^5$	$2.24 \cdot 10^6$	$1.13 \cdot 10^6$	0.51	-0.001
40	3.5	32.8	$1.17 \cdot 10^5$	$5.05 \cdot 10^5$	$5.31 \cdot 10^5$	1.05	-0.009
60	3.7	36.1	$1.12 \cdot 10^5$	$5.14 \cdot 10^5$	$4.77 \cdot 10^5$	0.93	-0.009

Table 7. Time required to reach viscosity plateau region (“steady-state gap height region”)

Time [min]	Temp [°C]	Viscosity [Pa·s]	G' [Pa]	G'' [Pa]	tan δ [-]	gap change [mm]
26	22	$6.63 \cdot 10^5$	$4.03 \cdot 10^6$	$1.06 \cdot 10^6$	0.26	-0.019
19	40	$2.34 \cdot 10^5$	$1.33 \cdot 10^6$	$6.14 \cdot 10^5$	0.46	-0.027
0	60	$2.40 \cdot 10^5$	$1.47 \cdot 10^6$	$3.57 \cdot 10^5$	0.24	-0.034

The onset of increase in viscosity was observed at a much earlier time and at a lower gap change at 22°C compared to 40°C and 60°C samples. This is because at 22°C, the resin system was

more solid-like (higher viscosity and lower $\tan \delta$), which would resist resin flow across the surface of the prepreg, resulting in a smaller gap change. At higher temperatures, the lower resin viscosity and higher $\tan \delta$ allowed for the increase in resin flow across the surface of the prepreg until it reached a critical gap height. As observed in Table 7, the time required to reach steady state gap height decreased with an increase in the temperature. At 60°C, the material reached the steady state gap height at 0 minutes, whereas the time it took to reach steady state gap height for 40°C was 19 minutes, and 26 minutes at 22°C. This suggests that the relative mobility of the resin was higher at 60°C compared to 40°C, where the actual resin viscosity in the prepreg system should have been lower at 60°C compared to the measured minimum viscosity at 40°C (Figure 18) assuming insignificant progression of the thermosetting reaction. This supports prior observations where the reduction of resin viscosity at higher temperatures allows the geometry to move closer to the fiber, and the increase in viscosity is an artifact induced by the measurement conditions.

An increase in complex viscosity and decrease in $\tan \delta$ from the critical gap height region to steady state gap height region was observed for all samples. A possible explanation for the decrease $\tan \delta$ could be due to the decrease in resin thickness as the geometry continues to lower towards the surface of the fiber, which effectively reduces G'' contribution to the system.^{24,64} The decrease in gap height could also be due to localized deformation of the fibers- where the decrease in gap height increases the packing density of the fiber between the tool-ply contact area, which effectively increases the G' of the system.⁶⁴ At the steady state gap height, the plateau in complex viscosity could indicate that the maximum resin distribution and/or fiber packing density is reached. The results suggest that the relative resin distribution and compressibility of the prepreg system is higher at a higher temperatures, as monitored by the

changes in gap height and viscoelastic properties. Since the friction between the two surfaces is highly dependent on the contact mechanism and the viscoelastic properties of the lubricating layer, a large decrease in gap height during the measurement interval could result in higher frictional values due the increase in resin distribution and contact between the tool-ply surfaces.

It is interesting to point out that differences in the initial prepreg gap height were observed for all samples, where a higher initial gap height corresponded to a higher initial viscosity. A common challenge with testing carbon fiber epoxy preregs is the difficulty of sample reproducibility due to variations in bulk properties of the as received material.⁵³ For example, surface variations due to differences in epoxy coverage, as well as structural variations due to sample location (e.g. twisted fiber samples obtained from the edges of the roll, compared to flat samples obtained from the middle of the roll) can have a direct impact on the measured properties.^{53,65} A top view of a cut section (120 x 90 mm) of the as-received prepreg is shown in Figure 19, with an uneven distribution of epoxy across the surface of the prepreg.

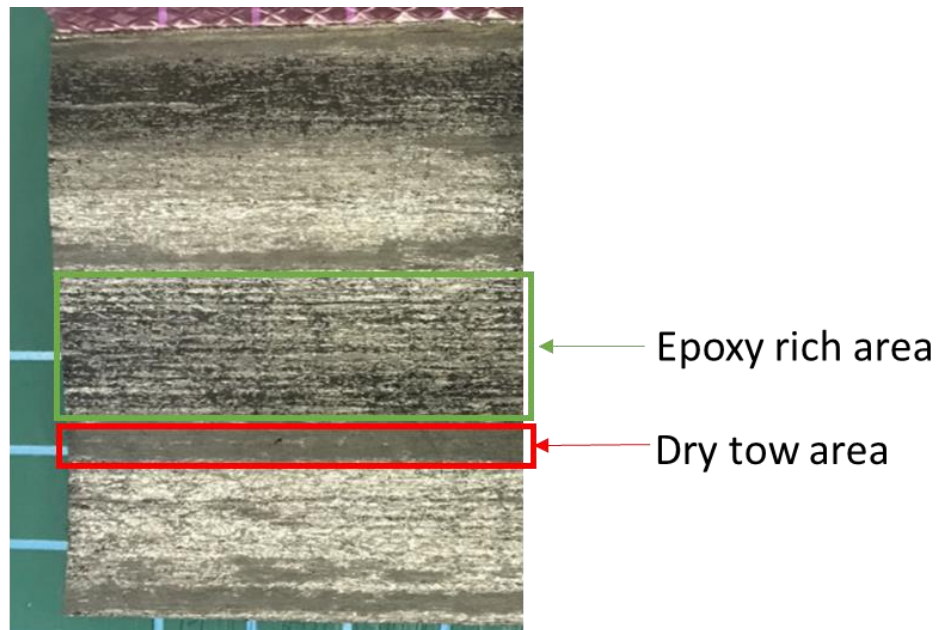


Figure 19. Top view of as received prepreg (HexPly M77/38%/UD300/50K) with varied resin coverage across surface (sample size 120 x 90 mm)

Because the rheological behavior of the prepreg is dependent on both the carbon fiber and epoxy matrix, the varied epoxy surface coverage will likely contribute to variabilities in measured results. A sample with a larger dry tow area is expected to have a lower initial gap height and complex viscosity as compared to a sample obtained from the resin rich area. In other words, consistent measurement and interpretation of the results would be dependent on the initial resin content available of the prepreg sample and the understanding of changes in resin distribution and/or contact mechanism between the tool-ply surfaces at various processing conditions.

4.1.3 Effects of Temperature on Resin Staging

The effects of temperature on resin staging were measured with a parallel plate geometry at 0.05 strain %, normal force 5N, cure temperatures of 90°C, 100°C, and 110°C and cure times of 120, 55, 24 minutes (respectively). The normal force of 5N was chosen based on the maximum forming pressure used for the tool-ply friction experiments. It should be noted that the storage modulus was normalized and converted to degree of conversion (α) using Equation 1. The purpose was to directly compare the cure behavior between samples, as difference in the viscoelastic properties were observed between samples due to surface variations (Shown in Figure 19). The overall results of the temperature as a function of resin conversion, α is shown in Figure 20 and Table 8.

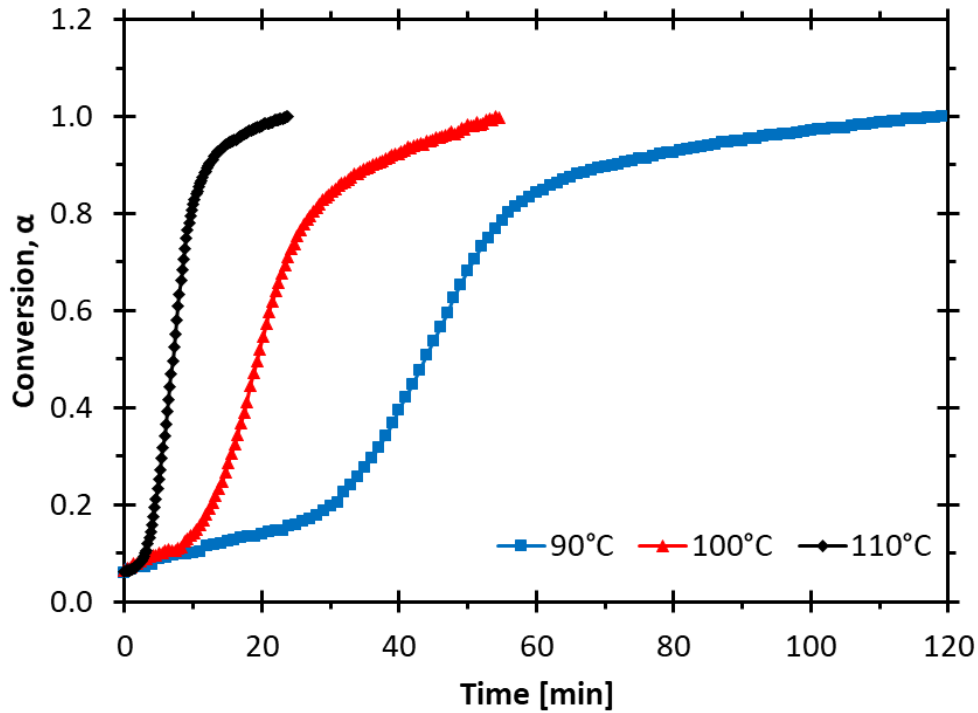


Figure 20. Effect of temperature on resin staging

Table 8. Degree of conversion at various cure temperatures

90°C		100°C		110°C	
α	time	α	time	α	time
[-]	[min]	[-]	[min]	[-]	[min]
0.05	0	0.06	0	0.06	0
0.26	34	0.25	14	0.25	5
0.51	44	0.50	19	0.50	7
0.75	53	0.75	25	0.75	9
0.99	109	0.99	51	0.99	20

A longer time was required to reach complete cure at 90°C compared to 110°C, which indicated materials cured at a higher temperature have a shorter forming time. The typical forming limit of an epoxy-amine system is determined at the gelation point at α of 0.5-0.7 (based on DSC and rheological measurements).^{40,53,54} As such, the time available for the frictional measurements over the cure intervals (based on α of 0.5) would be 44 minutes at 90°C, compared to 19 minutes at 100°C, and 7 minutes at 110°C.

4.1.4 Time Temperature Transformation (TTT)

The processing window for the lay-up and molding process with respect to the time, temperature, and resin staging was examined by determining the sub ambient glass transition temperature ($T_{g,sub}$), gel point (t_{gel}), vitrification (t_{vit}), and cure point (t_{cure}) as a function of the cure temperature. In theory, the material should be formed at or above the $T_{g,sub}$ and below t_{gel} .

The first point of interest with regards to processing prepreg materials is the sub-ambient glass transition temperature ($T_{g,sub}$). The $T_{g,sub}$ is synonymous to the glass transition temperature of a polymer in the transition from a glassy to rubbery state. The $T_{g,sub}$ definition is reserved for describing the transition behavior for uncured epoxy, as T_g of a prepreg is traditionally used to describe the glassy transition of the cured material for demolding purposes.⁵⁶ With regards to processing, the $T_{g,sub}$ is used to describe the material behavior to the layup process. Materials laid up below the $T_{g,sub}$ value could exhibit interfacial or brittle failure due to high viscosity and glassy state of the system compared to material processed close to $T_{g,sub}$ which can exhibit cohesive failure due to low viscosity (high tack).¹⁹

There are various methods in determining the $T_{g,sub}$, which can be quantified as the maximum of the G'' value or determined at the max $\tan \delta$.⁵⁶ The average $T_{g,sub}$ of the material with relevant viscoelastic parameters is shown in Table 9.

Table 9. Average $T_{g,sub}$ values of 3 samples heated at 10°C/min from 20°C, 1hz, and 0.05% strain

method	Time [min]	$T_{g,sub}$ [°C]	η^* [Pa·s]	$\tan \delta$ [-]
max G''	2.1±0.10	24±0.6	$6.77 \cdot 10^5 \pm 1.450 \cdot 10^4$	0.61±0.045
max $\tan \delta$	3.0±0.16	29±1.3	$2.57 \cdot 10^5 \pm 3.074 \cdot 10^4$	1.01±0.032

From Table 9, the $T_{g,sub}$ ranges from 24 ± 0.6 °C to 29 ± 1.3 °C depending on method of determination. The lower viscosity and higher $\tan \delta$ measured at 29°C suggest that the material will exhibit more viscous-fluid like behavior and be more formable compared to 24°C.

With regards to processing of thermosetting systems, the gelation point is of great interest as it is the temperature or time at which the resin transforms from a viscous liquid to an elastic gel.^{43,55,57,58} As discussed in section 3.3.3.5, various methods can be employed to determine the t_{gel} from rheological measurements. However, due to the lack of G' and G'' crossover point (Figure 15), and limited test conditions (one frequency), the t_{gel} in this study was determined based on the point at which the viscosity approaches infinity (Table 10), and at the point at which $\tan \delta$ drops suddenly (Table 11).

Table 10. Gel times determined at the point at which viscosity rises to infinity (0.05 strain %, normal force 5N, 1hz)

Temp [°C]	t_{gel} [min]	α_{gel} [-]	η^* [Pa·s]	G' [Pa]	G'' [Pa]	$\tan \delta$ [-]
90	28	0.18	$2.38 \cdot 10^5$	$1.41 \cdot 10^6$	$4.92 \cdot 10^5$	0.35
100	11	0.17	$2.26 \cdot 10^5$	$1.45 \cdot 10^6$	$4.78 \cdot 10^5$	0.34
110	3.4	0.12	$2.08 \cdot 10^5$	$1.28 \cdot 10^6$	$4.78 \cdot 10^5$	0.39

Table 11. Gel times determined with at which $\tan \delta$ drops suddenly (0.05 strain %, normal force 5N, 1hz)

Temp [°C]	t_{gel} [min]	α_{gel} [-]	η^* [Pa·s]	G' [Pa]	G'' [Pa]	$\tan \delta$ [-]
90	33	0.24	$2.91 \cdot 10^5$	$1.74 \cdot 10^6$	$5.72 \cdot 10^5$	0.33
100	12	0.19	$2.44 \cdot 10^5$	$1.45 \cdot 10^6$	$4.95 \cdot 10^5$	0.34
110	3.6	0.13	$2.18 \cdot 10^5$	$1.28 \cdot 10^6$	$4.92 \cdot 10^5$	0.39

The results showed that at the higher cure temperature, the time it took to reach critical gelation decreases. The α_{gel} was between 0.12-0.18 determined at the point where viscosity rises to

infinity, compared to a slightly higher α_{gel} between 0.13-0.24 determined at the point where $\tan \delta$ drops suddenly. The α_{gel} determined from both methods above were much lower than the α_{gel} reported in literature (0.5-0.7).^{37,40,53,54} Variations in the α_{gel} have been reported due to the measurement technique. For an epoxy-amine system, Mounif et. al.³⁷ found a higher α_{gel} of 0.7 obtained through DSC measurements compared to a lower α_{gel} of 0.58 determined through rheological measurements.³⁷ Differences in α_{gel} have also been reported due to the method of determination. For example, Sabzevari et al.⁶ studied the cure behavior of a unidirectional thermosetting epoxy prepreg system (IM7/977-2 UD, Cycom®) with a torsional rheometer (AR2000, TA Instruments). The author found an overall higher α_{gel} of 0.41 (determined at $\tan \delta = 1$), compared to α_{gel} of 0.38 (determined at the sudden drop of $\tan \delta$), and α_{gel} of 0.31 (determined at viscosity rise to infinity).⁶ The author concluded that the overall lower α_{gel} is likely due to the presence of the addition of a secondary curing agent (hardener) which altered the cure behavior of the resin system.⁶ As such, it is likely that the lower α_{gel} of the present system is due to the materials and methods used to determine α_{gel} . The α_{gel} should be examined at various frequencies (determined at the point at which $\tan \delta$ is independent of frequency), and at $G'' = G'$ (or $\tan \delta = 1$) for a more accurate description of the system.^{6,54}

The critical gelation time was determined using Equation 2 to estimate the gelation time at various temperatures.

$$t_{gel} = A \exp\left(-\frac{E}{RT}\right) \quad (2)$$

where t_{gel} is the time required to reach gelation at the isothermal condition, A is the pre-exponential factor, E is the apparent activation energy in $\text{kJ}\cdot\text{mol}^{-1}$, R is the universal gas constant in $(\text{kJ}\cdot\text{mol}^{-1}\text{K}^{-1})$, and T is the isothermal curing temperature in (K).^{37,55} The E and A values are

determined by plotting $\ln(t_{gel})$ against $1/T$ shown in Figure 21, with the corresponding parameters listed in Table 12.

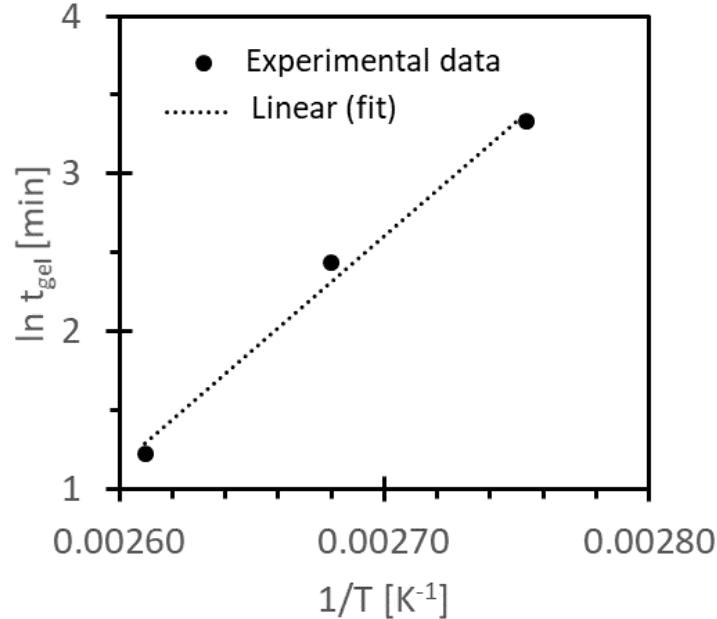


Figure 21. Critical gelation time at various cure temperatures determined by Arrhenius fit

Table 12. Corresponding parameters for determining gelation through Arrhenius fit

Method	E	A
[-]	[kJ·mol ⁻¹]	[min]
Onset of infinite viscosity	121.8	$8.87 \cdot 10^{-17}$
Sudden drop $\tan \delta$	128.0	$1.28 \cdot 10^{-17}$

A lower activation energy was observed for values determined at the infinite viscosity point compared to the value determined at the sudden decrease in $\tan \delta$. It should be noted that the calculated activation energy is much higher ($128 \text{ kJ} \cdot \text{mol}^{-1}$) than reported literature values of similar systems ($50\text{-}70 \text{ kJ} \cdot \text{mol}^{-1}$).^{6,41} A higher activation energy has been reported for systems that contains a secondary curing agent (harder), which requires a higher activation energy of reaction to initiate and complete cure of the system.⁶ However, while Equation 2 is typically used to describe the cure behavior of epoxy resin systems, the model is based on the assumption that the conversion (α_{gel}) is independent of the temperature.⁶ The α_{gel} of the present system

decreased with the increase in forming temperature (Table 10 and Table 11), this suggests that the gelation of the present system cannot be described by the Arrhenius fit shown in Equation 2. More complex models such as the Kamal and Sourour model should be used to develop a more accurate prediction of the gelation of the system.^{6,41,55}

Nevertheless, the results suggest that the limit of the forming conditions of the present system should be around α_{gel} of 0.19, and that the maximum available forming time of this prepreg at various temperatures can be approximated with the following equation: $t_{gel} = 1.28 * 10^{-17} exp\left(-\frac{128.0}{0.0083147T}\right)$, where T is the temperature in °C and t_{gel} is the critical gelation time in minutes.

The next processing parameter of interest is t_{vit} , which is the time it takes for the sample to transform from a rubbery gel to glassy gel.⁶ The vitrification point was determined by examining the maximum loss modulus (G'') at the isothermal cure conditions. The final parameter of interest is t_{cure} , which is the time it takes for a sample to reach full cure and is determined at the plateau of G' . The relevant viscoelastic properties at t_{vit} and t_{cure} are shown in Table 13 and Table 14.

Table 13. t_{vit} and relevant viscoelastic parameters determined various temperatures (0.05 strain %, normal force 5N, 1hz)

Temp [°C]	t_{vit} [min]	α_{vit} [-]	η^* [Pa·s]	G' [Pa]	G'' [Pa]	tan δ [-]
90	45	0.55	$5.35 \cdot 10^5$	$3.29 \cdot 10^6$	$6.83 \cdot 10^5$	0.21
100	20	0.57	$5.29 \cdot 10^5$	$3.25 \cdot 10^6$	$6.81 \cdot 10^5$	0.21
110	8	0.60	$6.00 \cdot 10^5$	$3.68 \cdot 10^6$	$8.32 \cdot 10^5$	0.23

Table 14. t_{cure} and relevant viscoelastic parameters determined various temperatures (0.05 strain %, normal force 5N, 1hz)

Temp [°C]	t_{cure} [min]	α_{cure} [-]	η^* [Pa·s]	G' [Pa]	G'' [Pa]	$\tan \delta$ [-]
90	99	0.97	$8.83 \cdot 10^5$	$5.54 \cdot 10^6$	$2.09 \cdot 10^5$	0.04
100	45	0.95	$8.47 \cdot 10^5$	$5.31 \cdot 10^6$	$3.72 \cdot 10^5$	0.07
110	18	0.97	$9.18 \cdot 10^5$	$5.75 \cdot 10^6$	$4.60 \cdot 10^5$	0.08

A modified TTT plot was constructed with the data collected from section 4.1.2 and section 4.1.3. The modified TTT plot was fitted with the predicted friction mechanisms described in the Stribeck curve (Figure 8) as a function of processing temperature and time (Figure 22), with a summary of the relevant viscoelastic properties shown in Table 15.

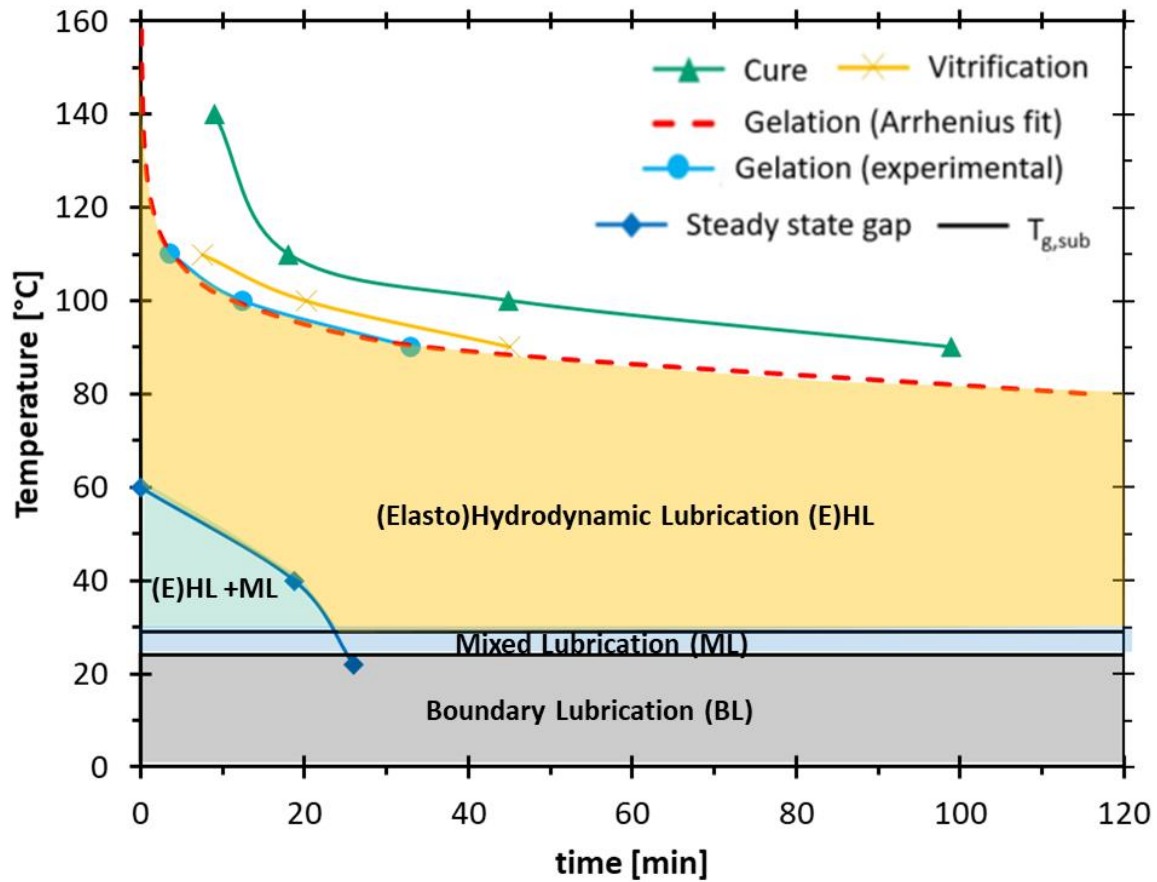


Figure 22. Modified TTT diagram

Table 15. Corresponding parameters for the modified TTT diagram

Region	Complex Viscosity [Pa·s]	$\tan \delta$ [-]	α [-]
below T_g	$9.88 \cdot 10^5$	0.16	0.06
$T_{g,sub,1}$	$6.77 \cdot 10^5$	0.61	0.06
$T_{g,sub,2}$	$2.57 \cdot 10^5$	1.01	0.06
Pre steady-state gap height	$1.15 \cdot 10^5$	0.99	0.06
Post steady-state gap height	$2.37 \cdot 10^5$	0.35	0.06
Gelation	$2.51 \cdot 10^5$	0.35	0.19
Vitrification	$5.55 \cdot 10^5$	0.22	0.58
Cure	$8.82 \cdot 10^5$	0.06	0.96

Below the $T_{g,sub}$, the surfaces should be separated by a thin resin film with high viscosity and ungelled-glass characteristics. This leads to the hypothesis that the system should exhibit friction mechanisms within the boundary lubrication (BL) regime. At temperatures above $T_{g,sub}$, the resin begins to soften, which should result in an increase in separation between the tool-ply surfaces, and the system should exhibit friction mechanisms in the mixed lubrication (ML) regime. At higher temperatures, the surfaces should be fully separated by a liquid-like resin layer which can support the movement between the tool-ply surfaces. As such, the system should exhibit friction mechanisms within the elasto-hydrodynamic (E)HL regime. While the measured viscoelastic properties above the steady state gap region were similar to the viscoelastic properties at the gelation line, the friction values measured at gelation should be higher due to the increase in network formation, which could resist deformation and movement between the tool-ply surfaces.

It is predicted that the material would exhibit friction mechanisms in both the ML and (E)HL lubrication regime below the steady state gap height region between 40-60°C due to variations in the resin distribution and contact mechanism between the tool ply surfaces. The

desirable forming range to minimize tool-ply friction should be within the (E)HL region above steady state gap height region and below the gelation line. It should be noted that these parameters used in the modified TTT diagram are approximate values, as measurements were conducted at a singular frequency (1hz), strain rate (0.05%), and normal force of 5N. More accurate values can be determined by examining the frequency and pressure dependence of the system.^{43,55,57}

4.2 Tool-Ply Friction

From the friction mechanism predicted from the modified TTT plot (Figure 22 and Table 15) the processing region with minimal friction forces should be in the E(HL) region (above the steady state gap height line, and below gelation line). The following sections discuss the impact of processing variables and prepreg staging history on the tool ply-friction.

4.2.1 Influence of Temperature on Tool-Ply Friction

In general, it has been observed that an increase in experimental temperature corresponds to lower frictional values due to the reduction in resin viscosity.^{5,59,66} However, deviations in the friction behavior have been reported in literature due to tool-ply contact at higher temperatures.^{5,24} An increase in the friction forces should be expected if the decrease in the gap height is greater than the critical gap height due to the increase in resin mobility and compressibility at higher temperatures that effectively increases the fiber dominated properties of the system (as described in Section 4.1.2). The effects of temperature on frictional sliding behavior are shown in Figure 23 with viscoelastic properties at corresponding temperatures measured at various gap heights (Table 16). It should be noted that the frictional force values were reported from the second iteration due to the long dwell time effects at low temperatures (discussed in subsequent section).

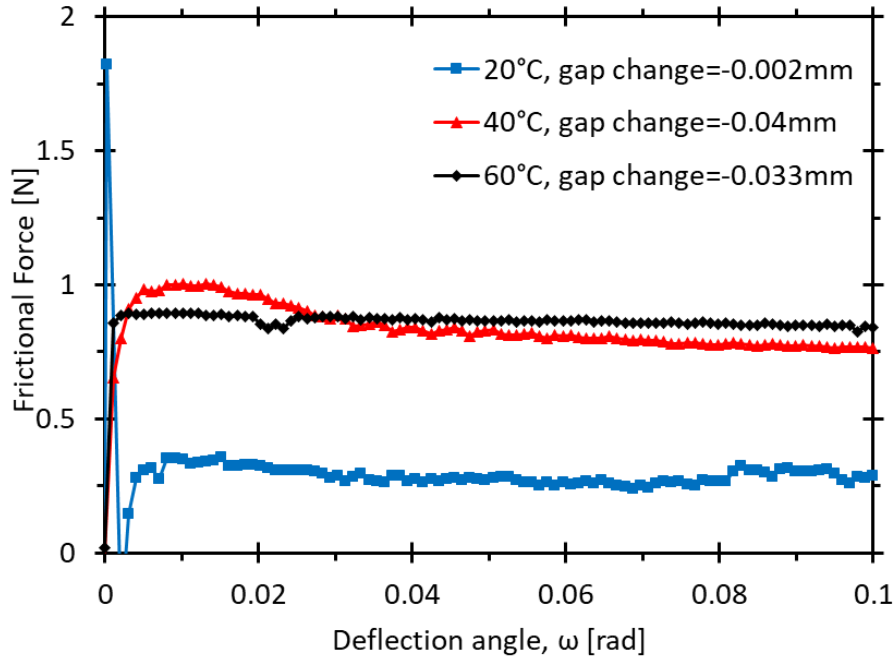


Figure 23. Frictional force vs. deflection angle at three temperatures (angular velocity 1mrad/s, normal force of 5N ($6.63 \cdot 10^4$ Pa)) *values reported from second iteration (with 200s dwell time)

Table 16. Viscoelastic properties measured from (1) high gap samples- SAOS at 0.05% strain, 1hz, heating rate of 10°C to 90°C (2) low gap samples- SAOS at 0.05% strain, 1hz, heating rate 10°C from 20°C to 40 or 60°C

Temperature [°C]	high gap			low gap		
	Viscosity [Pa·s]	$\tan \delta$ [-]	Gap change [mm]	Viscosity [Pa·s]	$\tan \delta$ [-]	Gap Change [mm]
20	$9.88 \cdot 10^5$	0.16	-0.001	$9.88 \cdot 10^5$	0.16	-0.002
40	$1.17 \cdot 10^5$	0.7	-0.003	$2.34 \cdot 10^5$	0.46	-0.027
60	$9.81 \cdot 10^4$	0.52	-0.01	$2.40 \cdot 10^5$	0.24	-0.034

At 20°C, the frictional force reached a peak value (F_s) and was immediately followed by a decrease and plateau region (F_k). The large F_s observed in the 20°C sample can be attributed to the long initial contact time and adhesive contributions (high viscosity) of the epoxy- where a large frictional force is required to “break” the bond formed between the epoxy and plate prior to bulk movement between the surfaces.^{18,24} This “stick-slip” behavior is characteristic of friction in the BL regime. At 40°C, the frictional force initially peaked, and gradually decreased until it reached a steady state value. The gradual decrease in the frictional forces is characteristic of frictional and viscous sliding behavior observed in the mixed lubrication (ML) regime. The lack

of distinct peak frictional value at 60°C is characteristic of viscous sliding behavior observed in the (E)HL regime. The changes in frictional sliding behavior at 40°C and 60°C are due to the decrease in resin viscosity at higher temperatures (shown from high gap samples in Table 16) which allows for an increase in resin distribution that acts as a lubricating layer between the surfaces.

In theory, the presence of the lubricating layer should reduce the friction between the surfaces due to the reduction in viscous resistance of the resin layer. Therefore, the F_k should be lower at 40°C and 60°C compared to 20°C. However, a larger F_k was observed at 40°C and 60°C compared to 20°C. The higher F_k at 40°C and 60°C may be associated with the increase in the compressibility and mobility of the prepreg at higher temperatures (as discussed in section 4.1.2). At higher temperatures, the reduction in resin viscosity allowed for an increase in resin distribution and decrease in the gap height between the tool-ply surfaces. As the gap height continued to decrease over the measurement interval, the higher resin mobility allowed for an increase in the localized fiber packing density, effectively increased the fiber dominated properties of the system, and the subsequent force required to move the geometry.^{5,24,67}

4.2.1.1 Data Repeatability

The relative contribution of initial contact time and wear of a sample was examined by repeating the frictional sliding test on the same sample. The experimental conditions were identical between each iteration, with the exception of varied initial contact time (due to the different time required for the heating/hold cycle at various temperatures) for the first iteration, and 200 second dwell time between subsequent tests. Data repeatability of a sample should be dependent in the contact mechanism and resin distribution at various contact temperature and times. An overall higher F_s/F_k ratio should be expected for the 20°C due to the higher viscosity of

the system. In addition, data repeatability should be expected at higher temperatures due to increased resin mobility observed at lower resin viscosities (Table 17).

The corresponding times required to reach steady state gap height region are shown in Table 17, where the frictional sliding values should remain relatively constant above the steady state gap height region or interval. The result of the frictional sliding test of samples at various experimental temperatures with multiple iterations is shown in Figure 24.

Table 17. Time required to reach steady state gap height at various temperatures for frictional sliding measurements

Isothermal Temperature [°C]	Time to reach steady state gap height [s]	corresponding interval for frictional sliding measurements [#]	steady state gap height [mm]
20	1560+	8	-0.019
40	1140	6	-0.027
60	0	0	-0.034

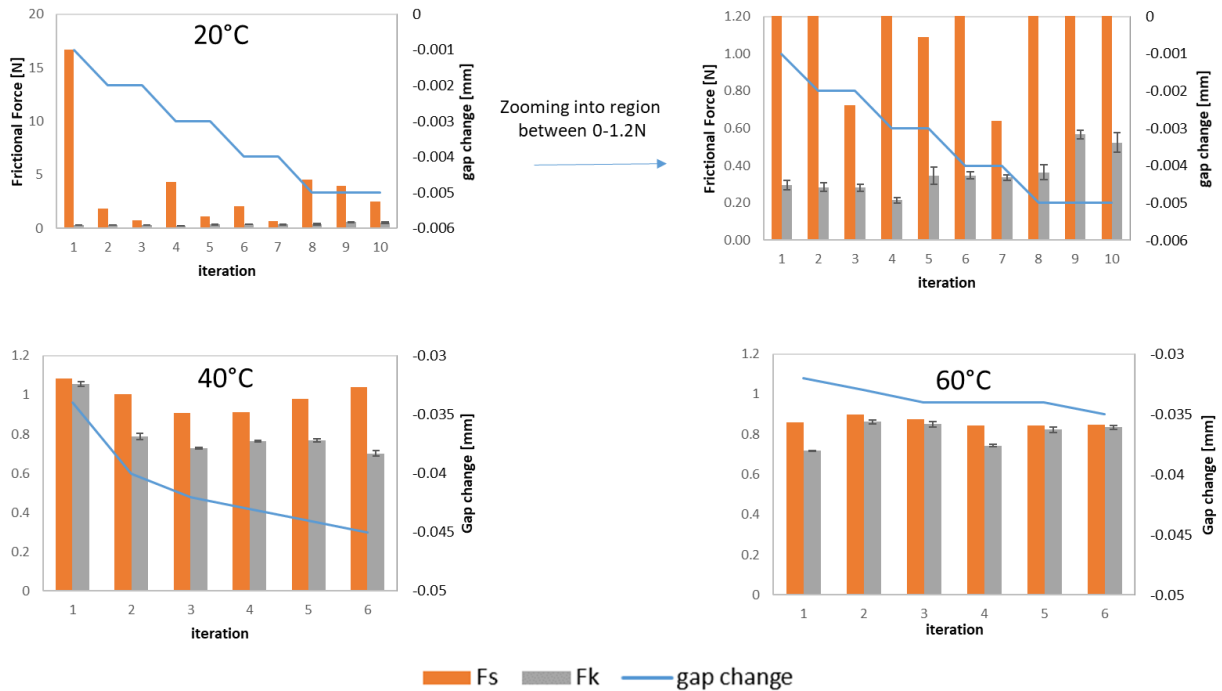


Figure 24. Changes in static and kinetic friction values measured various iterations at 20°C, 40°C, 60°C (rotational velocity of 100mrad/s and normal force of 5N (contact pressure of $6.63 \cdot 10^4$ Pa))

A large decrease in F_s between interval 1 and 2 for 20°C was due to increase in bond formation promoted by the longer dwell time ($t_{0,1}= 800s$, $t_{0,2}=200s$). In addition, a decrease in F_s was observed at constant gap heights, whereas changes in the frictional forces were observed over the measurement interval up to the predicted steady state gap height interval (due to the closer proximity of the critical gap height of -0.009mm). A larger variation between F_s was observed in the 20°C sample compared to the 40°C and 60°C sample. This could be due to the lower resin viscosity at higher temperatures, which allows for the resin to relax/flow back between the geometry test between each interval. The result indicates that a sample at a lower testing temperature is more sensitive to repeated tests compared to samples at a higher testing temperature.

4.2.2 Influence of Velocity on Tool-Ply Friction

The effects of sliding velocity on the frictional sliding behavior of 40°C and 60°C were examined using a 1 mm ring geometry with a normal load of 5N. Frictional sliding results are shown in Figure 25. It should be noted that the frictional force values are reported from the second iteration due to variations in the initial contact time (discussed in the previous section).

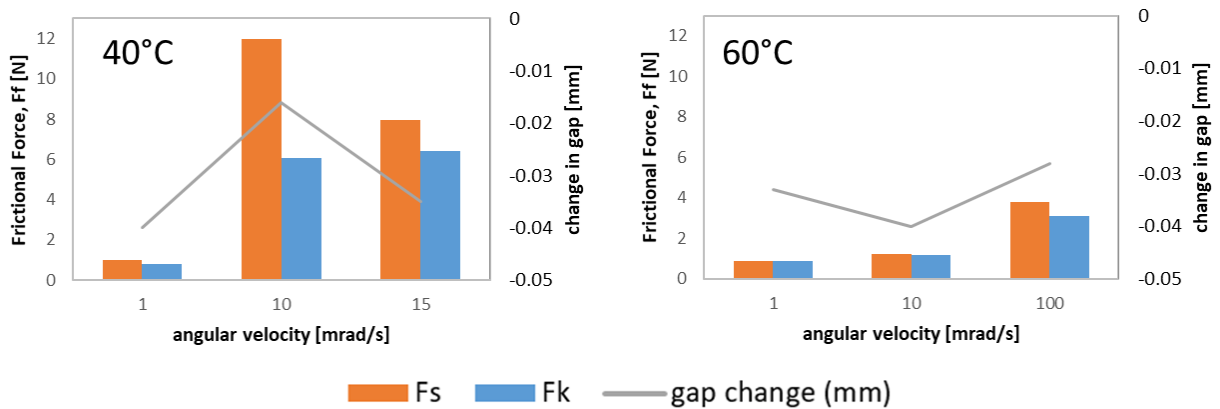


Figure 25. Frictional force vs. angular velocity for 40°C, 60°C samples (normal force of 5N)
 *values reported from second iteration (with 200s dwell time)

At 60°C, an increase in F_f was observed with an increase in sliding velocity, which is consistent with the behavior observed in the transition region between ML and (E)HL regime and in the (E)HL regime.^{5,18} Changes in sliding behavior from viscous to a combination of viscous and frictional sliding behavior is observed from the low sliding velocity of 1-10 $\text{mrad}\cdot\text{s}^{-1}$ to the high sliding velocity 100 $\text{mrad}\cdot\text{s}^{-1}$. This suggests that the friction mechanism of the system can be changed by altering the tooling velocity. At 40°C, an increase in F_f was observed with an increase in sliding velocity from 1 to either 10 or 15 $\text{mrad}\cdot\text{s}^{-1}$. Compared to 60°C, the frictional force at 40°C initially peaked, and gradually decreased until it reached a steady state value due to the increase in viscous contribution of the prepreg at the lower temperature.

While the F_f was expected to increase with an increase in sliding velocity, the F_s was larger at 10 $\text{mrad}\cdot\text{s}^{-1}$ compared to at 15 $\text{mrad}\cdot\text{s}^{-1}$ at 40°C. The variation of F_f could be due to differences in resin distribution as shown in Figure 19, where samples obtained from a dry tow area corresponded to a lower initial gap height and higher complex viscosity compared to samples obtained from a resin rich area. Since the initial gap height of the 1 $\text{mrad}\cdot\text{s}^{-1}$ and 15 $\text{mrad}\cdot\text{s}^{-1}$ samples were higher (0.419 and 0.415mm, respectively) compared to the lower initial gap height of the 10 $\text{mrad}\cdot\text{s}^{-1}$ sample (0.345mm), the higher F_s of the 10 $\text{mrad}\cdot\text{s}^{-1}$ could be due to the increase in tool-fiber contact in the dry tow area.

4.2.3 Influence of Pressure on Tool-Ply Friction

The effects of normal force on the frictional sliding behavior of 40°C were examined using a 1 mm ring geometry with a sliding velocity of 10 $\text{mrad}\cdot\text{s}^{-1}$. Frictional sliding results are shown in Figure 26.

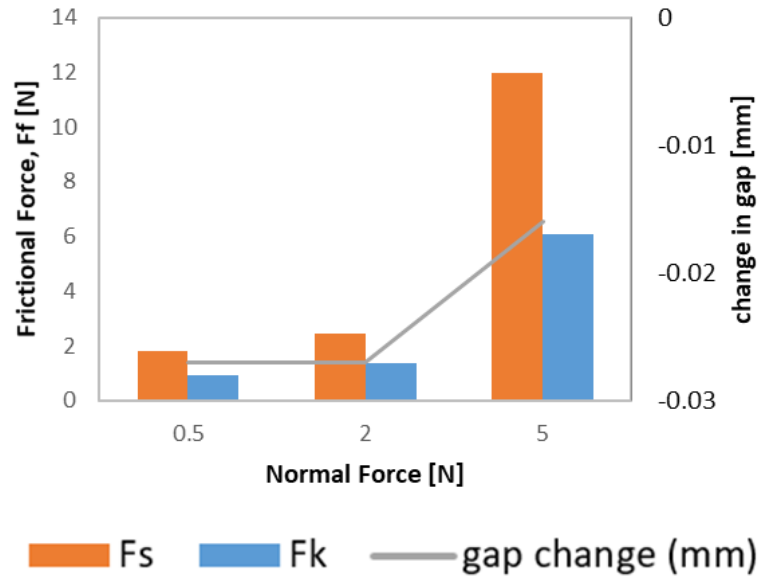


Figure 26. Frictional force at normal forces of 0.5, 2, 5N (contact pressure of $6.63 \cdot 10^3$, $2.65 \cdot 10^4$, $6.63 \cdot 10^4$ Pa, respectively) (40°C , angular velocity $10\text{rad}\cdot\text{s}^{-1}$) *values reported from second iteration (with 200s dwell time)

An overall increase in F_f was observed with an increase in normal force from 0.5-5N, which is consistent with behavior observed in the transition region between ML and E(HL) regime.⁶⁸ The non-linear increase of frictional force suggests that the frictional dependence of the present system does not obey Amonton's Law described in equation 3, as this law is typically used to describe friction behavior of non-adhering surfaces.^{59,69} This is because for a non-adhering surface, the surface roughness and contact area between the asperities remains constant at different pressures. Therefore, the friction forces increases linearly with increases in applied pressure.¹⁸ However, changes in gap height were observed in the present system, suggesting that the resin distribution and the true contact area between the surfaces could be non-constant over the measurement interval. The load dependence of the present system could be better described by a contribution of the adhesion forces and applied load; where adhesive contribution is higher at low loading forces, and lower at high loading forces.⁶⁹

4.2.4 Influence of Temperature on Sample Deformation

The differences in measured F_f and complex viscosity from rheological results reported thus far were made on the assumptions that a large decrease in gap height would result in an increase in fiber-tool contact. Therefore, the effects of experimental temperature on subsequent sample “morphology” was examined under an OMAX microscope with 4x objective (Figure 27). From the top view images, a visible ring outline could be seen in the 40°C and 60°C compared to the 20°C sample. This presence of the ring geometry at higher temperatures suggests that the effective increase in viscosity (Figure 18) and higher friction values (Figure 23) observed at 40°C and 60°C was due to the increase in resin distribution and localized fiber packing density that increases the contact between the tool-fiber surfaces. In addition, the magnified top view of the samples showed fiber misalignment in the 40°C sample and not in the 60°C sample, suggesting that fiber misalignment is caused by the lower gap height and higher viscosity of the 40°C sample (see Table 16).

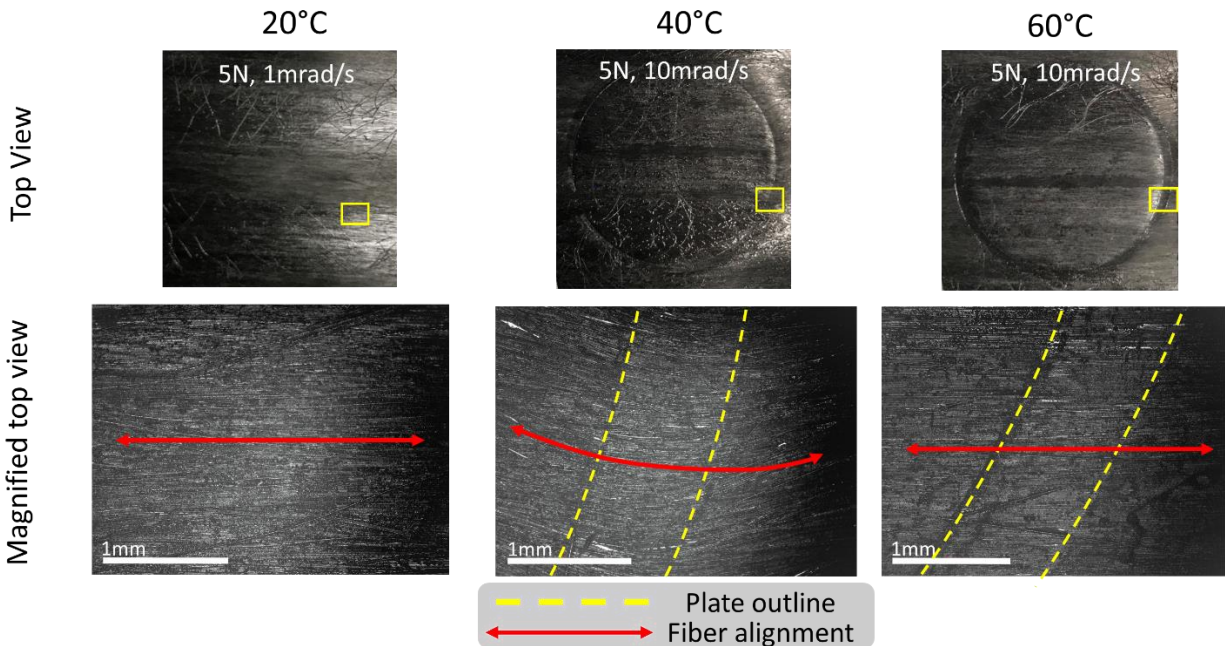


Figure 27. Top view and microscope images of samples after frictional sliding tests

The imaging results can be further compared with the measured rheological results shown in Table 18. Prior literature has suggested that the likelihood of fabric distortion can be predicted by the F_s/F_k ratio.⁷⁰ In general, static friction is considered as friction between non-moving surfaces, and is dominated by adhesion between the contact surface asperities, the time and mode of contact, whereas the kinetic friction is described by the friction between two moving surfaces and is dominated by the viscoelastic properties of the materials.⁵ When the F_s/F_k is approximately equal to 1, the material should exhibit viscous sliding behavior in the (E)HL regime. When F_s/F_k greater than 1, the material is likely to exhibit a combination frictional sliding and viscous sliding behaviors, typically observed in the ML regime. It should be noted that while the F_s/F_k ratio was large for the 20°C sample, fabric distortion was not observed, due to the high viscosity and glass-like characteristics of the material.

Table 18. Summary of experimental results from various techniques

Temp [°C]	SAOS		Sliding Friction				Imaging	
	η^* [Pa·s]	$\tan \delta$ [-]	gap change [mm]	F_s [N]	F_k [N]	F_s/F_k [-]	Ring outline? [-]	Fiber distortion? [-]
20	$9.88 \cdot 10^5$	0.16	-0.002	1.82	0.28	6.4	No	No
40	$1.17 \cdot 10^5$	0.7	-0.016	11.99	6.08	1.97	Yes	Yes
60	$9.81 \cdot 10^4$	0.52	-0.04	1.24	1.2	1.03	Yes	No

4.2.5 Influence of Resin Staging on Tool-Ply Friction

With regards to thermoset forming process, it generally recommended that the pressure should be applied at or near the minimum viscosity and maintained up to the gelation point to ensure proper wetting and consolidation.⁴² Since increases in friction forces have been observed near the gelation point, this suggests that movement of the tool near gelation point could be significant in defect formations during the forming process.^{29,30}

From the results determined in Section 4.1.3, the material should exhibit friction mechanisms in (E)HL region at the onset of experiment. As the material begins to cure, the

friction should increase up to the gelation point at α of 0.19. Frictional measurements were collected under a range of tooling conditions listed in Section 3.3.4. Due to surface variations observed in samples (Figure 19) a single sample was used to examine the frictional sliding behavior over the cure interval. Samples were heated from 20°C to the desired temperature at 10°C·min⁻¹. Frictional sliding measurements were made every 301 seconds (sliding time 10 seconds followed by 291 seconds rest time between intervals). Staging of the sample was calculated with spline fitting (in MATLAB) the measurement time with the staging time determined from section 4.1.2. The influence of resin staging on the frictional sliding behavior is shown in Figure 28 and Figure 29.

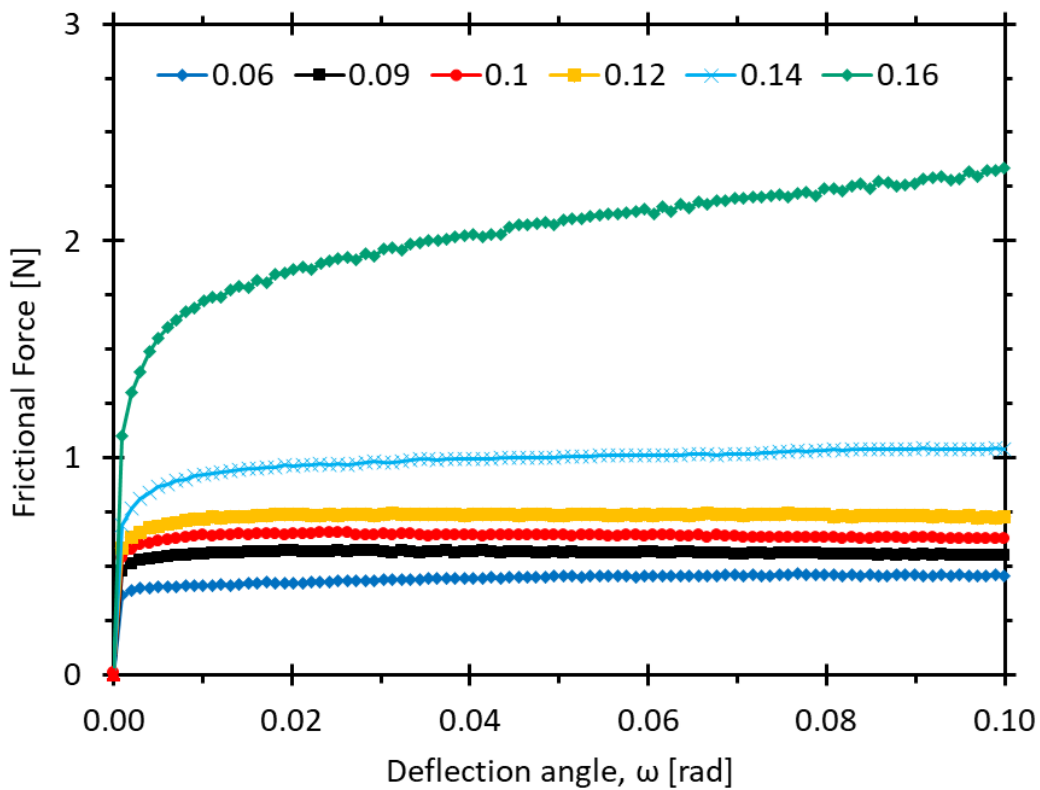


Figure 28. Frictional force vs. deflection angle from α 0.06 to 0.16. (90°C, angular velocity 10rad/s, normal force of 5N ($1.02 \cdot 10^4$ Pa), rest time of 291s per interval)

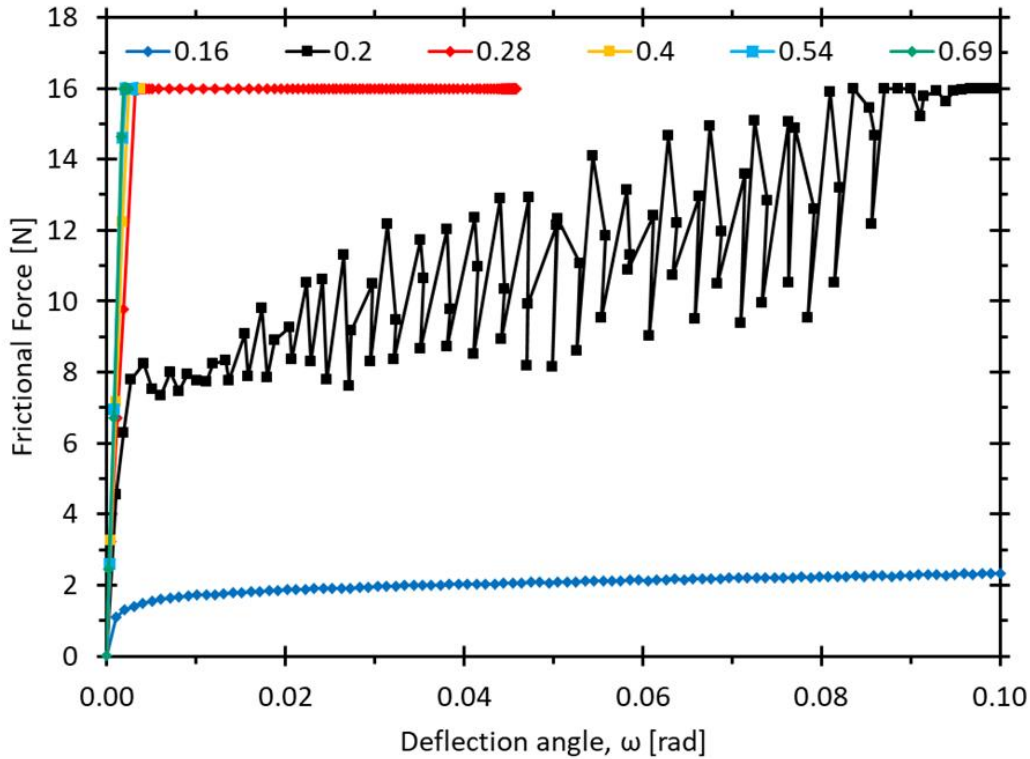


Figure 29. Frictional force vs. deflection angle from α 0.16 to 0.69. (90°C , angular velocity $10\text{mrad}\cdot\text{s}^{-1}$, normal force of 5N ($1.02\cdot 10^4\text{ Pa}$), rest time of 291s per interval)

A gradual increase in the frictional force (F_f) was observed from low resin staging intervals between α of 0.06-0.14. In this region, the F_f increased and leveled off without a distinct peak value, which is characteristic of viscous sliding behavior observed in the (E)HL regime. The increase in F_f over the staging interval is due the increase in network formation and viscosity at higher α . A change in frictional sliding behavior was observed at α of 0.16, where the friction force continued to increase over the measurement interval. This is because the system is near critical gelation point at α of 0.19 (determined in section 4.1.3), where the increase in network formation dramatically increases the viscous resistance between the two surfaces. At α of 0.2, the frictional force increased over the measurement interval, and exhibited “stick-slip” behavior. This is because beyond the gelation point, the material is in a rubbery-gel state, and it could be possible to have movement between the tool-ply surfaces. However, as the material continues to

cure, the stick slip behavior increases due to drastic increase in crosslink density and the adhesive forces between the tool-ply surfaces. Beyond α of 0.28, the friction forces increased linearly and plateaued at 16 N due to torque limitations of the instrument. The results are consistent with friction limitations reported in literature, where a sharp increase in frictional forces is observed near the gelation point of a resin system.^{29 30}

It was hypothesized that fiber deformation should be present near the gelation point due to the significant increase in F_f and stick-slip motion observed in Figure 29. A top view of the sample (Figure 30) showed the presence of prepreg distortion after the experiment. However, the extent of fiber deformation could not be determined by the method discussed in section 4.2.4 since the prepreg was cured onto the plate after the experiment. Nonetheless, the results suggest that tooling near or above the gelation point should be avoided to minimize manufacturing defects.



Figure 30. Top view of cured prepreg after frictional sliding experiment

4.3 Description of Overall Friction behavior in Thermosetting Prepreg Systems

Since friction mechanisms observed are in the mixed lubrication regime, the results presented here suggest that the friction behavior of this prepreg system cannot be described by Amontons's law for non-adhering surfaces. Therefore, the friction behavior can then be more accurately described as a contribution of adhesive and load forces with Equation 13.⁶⁹

$$F_f = \sigma A + \mu F_N \quad (13)$$

where F_f is the frictional force, σ is the critical shear stress, A is the real contact area, μ is the coefficient of friction, and F_N is the normal load applied on the object.⁶⁹ Since the σ term describes the force required to break the intermolecular bonds formed between the surfaces, this suggests the friction forces would be more sensitive to changes in the contact area, which can be monitored by the changes in gap height. In addition to changes in contact area, the system would also be more sensitive to changes in degree of cure due to the increased adhesive forces as the cure progresses. The increase in cure of the system effectively increases the number of bonds formed per unit area, which increases the critical shear stress required to “break” the bonds prior to sliding. Thus, as the cure progresses in the system, the F_f should increase until a critical point at which the critical shear stress required to break the bonds exceeds the limitations of the machine. This behavior would explain the large increase in F_f observed near the critical gelation point.

4.3.1 Proposed Friction Map

The results presented here suggest that friction during a thermoset prepreg composite forming process is dependent on a set of processing parameters including temperature, pressure, sliding velocity, and resin staging. Since the friction between two surfaces is highly dependent on the contact mechanism and the viscoelastic properties of the lubricating layer, changes in gap height and the F_s/F_k ratio are used to qualitatively describe the contact mechanism and sliding behavior expected at various processing conditions, as shown in the proposed friction map in Figure 31.

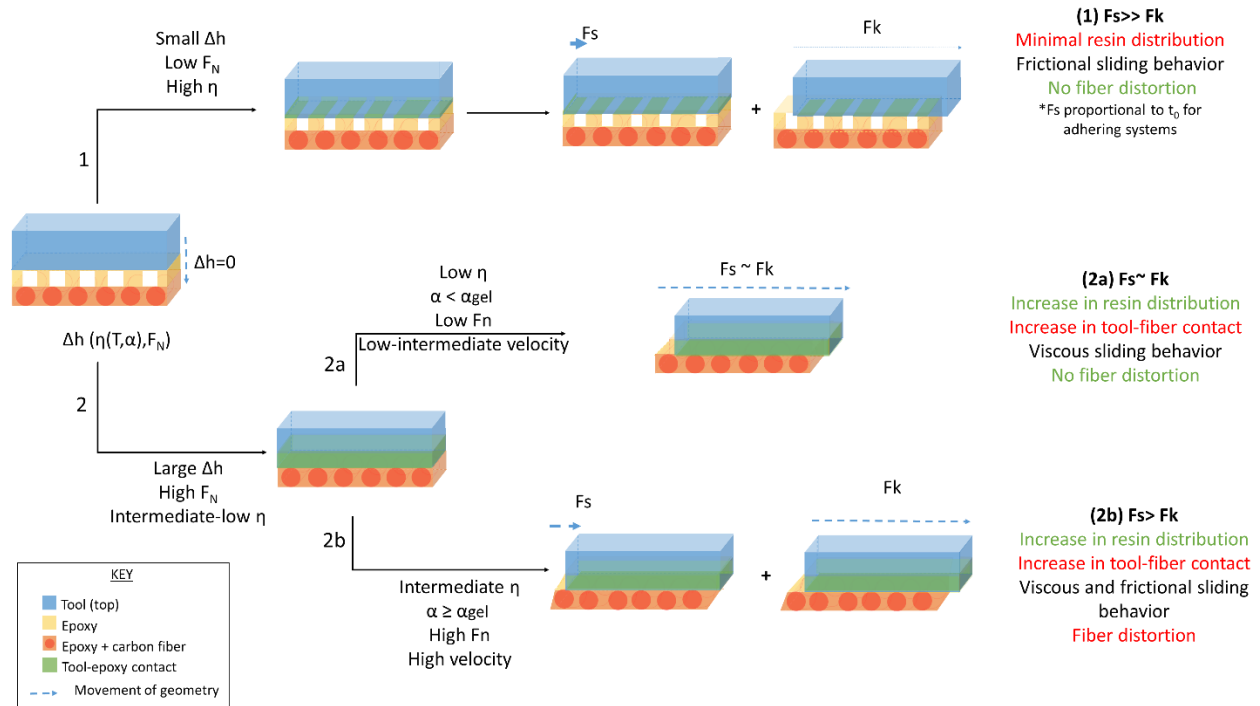


Figure 31. Proposed friction map

At low temperatures (such as below $T_{g,sub}$ of 24°C shown in modified TTT diagram in Figure 22), the material would have a high resin viscosity and ungelled-glass characteristics, which would resist deformation resulting in a lower change in gap height (Δh) and lower resin-tool contact area (path 1). The fiber-tool surface is separated by the solid-like resin layer, where a large frictional force (large F_s) is required to “break” the bond formed between the resin-plate contacting regions prior to bulk movement between surfaces (F_k). In this region, the system should exhibit friction mechanisms within the boundary lubrication (BL) regime, and the sliding behavior is characterized by a very high F_s/F_k ratio with no fiber distortions.

At higher temperatures, the reduction in resin viscosity allowed for an increase in resin distribution across the tool-ply surface, resulting in a larger change in gap height, and larger resin-tool contact area (path 2). While the presence of the lubricating resin layer should reduce the friction between the tool-ply surfaces, the reduction in the resin viscosity at the higher temperatures allowed for an increase in resin mobility and compressibility of the fibers. As the

gap height continues to decrease over the measurement interval (between the critical gap and steady state gap height interval shown in Figure 18), the localized fiber packing density increases (ring outlines shown in Figure 27), which effectively increases contact between the tool-fiber interface and the subsequent force required to move the geometry (Figure 23). The sliding behavior in region 2 is dependent on the resin viscosity and true contact area between the surfaces.

At a lower resin viscosity (path 2a), the surfaces are fully separated by a liquid-like resin layer which can support the movement between the tool-ply surfaces. As such, the system should exhibit friction mechanisms within the elasto-hydrodynamic (E)HL regime, and the sliding behavior is characterized by a F_s/F_k of approximately 1 (Figure 23) with no fiber distortions (Figure 27). This is compared to samples with an intermediate resin viscosity (path 2b), where the combination of the fiber-tool contact (at the lower gap height) and viscous resistance of the resin layer would likely result in frictional and viscous sliding behavior, characterized high F_s/F_k ratio (Figure 23) with fiber distortions (Figure 27). Similar behavior would be expected to be observed close to the gelation point of the material due to high adhesion contributions.

While the results suggests that the increase of F_f and the cause of fiber deformation between the tool-ply surfaces at higher temperatures is a contribution of the increased resin distribution and compressibility of the tool-ply system at the lower gap heights (Figure 27), the relative contact and friction contributions between the resin layer and fiber contact remains unclear. Specifically, this is due limited sample size, and variations in resin distribution of the prepreg material (Figure 19), which contains varied regions of resin rich and deficient areas. This contributes to differences in initial viscosity (Figure 18) and variations in the measured frictional

forces (Figure 25). As such, additional measurements should be conducted to distinguish between frictional and viscous sliding contributions.

CHAPTER 5

CONCLUSIONS AND FUTURE RECOMMENDATIONS

5.1 Conclusions

In this study, a torsional rheometer was used to investigate the effects of processing parameters such as temperature, velocity, normal force, and cure on the tool-ply friction of a UD carbon fiber epoxy prepreg. The viscoelastic properties and cure characteristics of the material were measured with dynamic rheological analysis. Rheological results were compared to the reported cure behavior of the neat resin because resin samples are rarely available for testing when obtaining prepreg materials from a manufacturer. The minimum viscosity (η^*_{\min}) of the prepreg system was found to be on average five orders of magnitude larger than the η^*_{\min} of the neat resin system due to the presence fiber in the prepreg. A much lower temperature required to reach the minimum viscosity ($T_{\eta^*_{\min}}$) of 40°C was found for the prepreg system compared to the $T_{\eta^*_{\min}}$ of 108°C the neat resin system. While deviations in minimum viscosity can be due sample aging and sample variabilities, the inconsistencies may also be a result of measurement conditions.

Isothermal tests below cure temperature, ranging from 22°C-60°C, showed that the complex viscosity of the system is dependent on time, temperature, and pressure due to increase in contact area and closer proximity to the fiber surface. Increase in complex viscosity is observed at a critical gap height change of -0.009 mm, with the plateau of complex viscosity at the steady state gap height region. At higher temperatures, the decrease in resin viscosity allows for an increase in the resin mobility and compressibility of the system, resulting in the larger

decrease in gap height and effective increase in the G' of the system. The results suggest that the increase in viscosity is an artifact induced by the measurement conditions.

A time-temperature-transformation diagram was established to examine the preliminary processing parameters for a compression molding process. Isothermal cure experimental data ranging from 90-110°C were used to determine the sub-ambient glass transition temperature ($T_{g,sub}$), gel point (t_{gel}), vitrification point (t_{vit}), and cure point (t_{cure}). The t_{gel} of the system at various cure temperatures can be found by using the following equation: $t_{gel} = 1.28 * 10^{-17} \exp(-\frac{128.0}{0.008314T})$, where T is the temperature in minutes, and t_{gel} is the critical gelation time in minutes. At regions below the $T_{g,sub}$ and above cure lines, the material would exhibit solid-like properties with high viscosity values. In the region between vitrification and the gelation line, the material should behave like a rubbery gel. A modified TTT diagram was constructed to predict the frictional sliding behavior at the various processing time and temperatures. Suitable processing parameters for molding would be between the steady state gap and below the predicted gelation line, where the $\alpha_{gel}=0.19$ and $\eta^*_{gel}=2.5*10^5 \text{ Pa}\cdot\text{s}$ and $\eta^*_{steady\ state\ gap}=2.37\cdot 10^5 \text{ Pa}\cdot\text{s}$.

Frictional sliding results showed that an increase in experimental temperature results in increase in F_f due to the lower gap height and contact between the tool-ply surfaces. An increase in velocity resulted in increase in F_f , and an increase in normal force resulted in an overall increase in F_f . The frictional sliding behavior was observed to be in the transition region between mixed lubrication (ML) and elasto-hydrodynamic (E)HL regime. Results suggest that the friction behavior of the prepreg system is dependent on the adhesion and friction interaction at the surfaces. Therefore, changes in gap height has a significant effect on the friction behavior due to variations in contact area and contact mechanism between the surfaces. Fabric deformation and

distortion was observed in magnified views of the samples, suggesting that imaging results can be coupled with rheological measurements to verify the effects of processing parameter on prepreg distortion. In addition, the results indicated that the increase in F_f observed at higher temperatures is due to the increase in fiber dominated properties observed at the lower gap heights. The relative gap change can be correlated to resin viscosity, and the likelihood of fabric distortion can be described by the F_s/F_k ratio, where a large ratio will result in fabric distortion.

The effects of cure stage on the frictional sliding behavior at various processing conditions was examined with a parallel plate geometry. Results showed an increase in μ as the sample cures, with a sharp increase at α of 0.16 which is lower than the predicted α_{gel} of 0.19 determined from TTT measurements. Results suggest that change in degree of cure has a significant effect on friction, as increasing cure effectively increases adhesion between the two surfaces. Fabric deformation was observed in samples after the experiments, however, the extent of fiber deformation could not be verified since samples were cured onto the plates during the experiment.

The overall results indicate that the friction behavior of the thermosetting prepreg system is dependent on the contribution of adhesive and load forces, where the frictional sliding behavior between the tool-ply systems can be controlled by altering the processing parameters. A modified TTT diagram was developed to predict the frictional sliding regimes with respect to changes in the viscoelastic properties as a function of time, temperature, and contact mechanism predicted by the changes in gap height. The frictional sliding results are consistent with behaviors observed in literature, which suggest that the rheometer can be used to characterize frictional sliding behavior of thermosetting prepreg systems. However, variations in the frictional sliding behavior can be expected due to the changes in contact area and contact mechanism

observed at different gap heights. In addition, a frictional map was constructed by combining the results from the viscoelastic, frictional, and surface analysis of the samples, where a combination of the viscoelastic behaviors and measurement conditions such as changes in gap height, and the static and kinetic friction ratio can be used to predict the tool-ply friction mechanisms.

5.2 Recommendation for Future Studies

While this research has provided insight in characterizing tool-ply friction as a function of changes in the viscoelastic properties at various processing conditions with a commercial rheometer, certain areas of improvement can be made to improve the understanding of the friction mechanisms. Since the overall results suggest that friction mechanisms of the tool-ply system are a combination of adhesion and friction forces, it would be of interest to quantify changes in the contact area and fiber distortion as a function of temperature and gap height. Such data could provide an additional understanding on the adhesive contributions and contact mechanism between the tool-ply surfaces in frictional measurements. In addition, the average resin distribution of the material should be examined to account for the variation in the resin distribution of the as received prepreg material.

While the modified TTT plot provided insight on the friction formation associated with the composite forming process, additional analysis such as time temperature superposition can provide a broader understanding on the frictional response at various frequency and shear rates. In addition, the α_{gel} should be further examined at various experimental conditions (such as different frequencies and pressure) and should be predicted with more complex models to develop a more accurate description of the processing window of the present system.

REFERENCES

1. Federal Aviation Administration (FAA). in *Aviation Maintenance Technician Handbook-Airframe, Volume 1* 592 (Aviation Supplies and Academics, Inc., 2012).
2. Pansart, S. in *Advanced fiber-reinforced polymer (FRP) composites for structural applications* 144–154 (Woodhead Publishing Limited, 2013).
doi:10.1533/9780857098641.2.125
3. Bai, J. *Advanced fiber-reinforced polymer (FRP) composites for structural applications*. (Woodhead Publishing Limited, 2013).
4. Costa, M. L., Rezende, M. C., de Paiva, J. M. F. & Botelho, E. C. Structural Carbon/Epoxy Prepregs Properties Comparison by Thermal and Rheological Analyses. *Polym. Plast. Technol. Eng.* **45**, 1143–1153 (2006).
5. Harrison, P., Thije, R. ten, Akkerman, R. & Long, A. C. Characterizing and Modelling Tool-ply Friction of Viscous Textile Composites. **7**, 5–22 (2011).
6. Sabzevari, S. M. Cure Kinetics and Process Modeling of a Carbon-Fiber Thermoplastic-Toughened Epoxy Resin Prepreg. (Wichita State University, 2010).
7. Brostow, W., Kovacevic, V. & Vrsaljko, D. Tribology of polymers and polymer-based composites. *Joyrnal Mater. Educ.* **32**, 18 (2010).
8. Das, R. Stress Relaxation Behavior of Carbon Fiber-Epoxy Prepreg Composites During and After Cure. (Wichita State University, 2008).
9. Ashby, M. F. *Materials Selection in Mechanical Design*. (Butterworth-Heinemann, 1999).
10. Jones, R. M. *Mechanics of Composite Materials*. (Taylor & Francis Group, LLC, 1999).
11. Gowayed, Y. in *Developments in Fiber-Reinforced Polymer (FRP) Composites for Civil Engineering* 1–17 (Woodhead Publishing Limited, 2013).
doi:10.1533/9780857098955.1.3
12. Campbell, F. C. *Structural Composite Materials*. (ASM International, 2010).
13. Hull, D. & Clyne, T. W. *An Introduction to Composite Materials*. (University Press, Cambridge, 1996).
14. Harper, L. T., Turner, T. A., Martin, J. R. B. & Warrior, N. A. Fiber Alignment in Directed Carbon Fiber Preforms- A Feasibility Study. *Compos. Mater.* **43**, 57–74 (2009).
15. Fiore, V. & Valenza, A. in *Advanced fiber-reinforced polymer (FRP) composites for structural applications* 88–121 (Woodhead Publishing Limited, 2013).
doi:10.1533/9780857098641.1.88
16. Bair, H. E. *et al. Thermal Characterization of Polymeric Materials*. (Academic Press, Inc., 1981).
17. Elkington, M. *et al. Hand layup : understanding the manual process. Adv. Manuf. Polym.*

- Compos. Sci.* **1**, 138–151 (2015).
18. Sun, J., Li, M., Gu, Y., Zhang, D. & Li, Y. Interply friction of carbon fiber / epoxy prepreg stacks under different processing conditions. *J. Compos. Mater.* **48(5)**, 515–526 (2014).
 19. Crossley, R. J., Schubel, P. J. & De Focatiis, D. S. A. Time-temperature equivalence in the tack and dynamic stiffness of polymer prepreg and its application to automated composites manufacturing. *Compos. Part A Appl. Sci. Manuf.* **52**, 126–133 (2013).
 20. Putnam, J. W., Seferis*, J. C., Pelton, T. & Wilhelm, M. Perceptions of Prepreg Tack for Manufacturability in Relation to Experimental Measures. *Sci. Eng. Compos. Mater.* **4**, 143–154 (1995).
 21. Crossley, R., Schubel, P. & Warrior, N. The experimental characterisation of prepreg tack. *17th Int. ...* (2009).
 22. Lennon, J. J. & Mallon, J. Surface friction effects related to pressforming of continuous fibre thermoplastic composites. *Compos. Manuf.* **6**, 169–175 (1995).
 23. ASTM International. *ASTM D1894-14- Standard Test Method for Static and Kinetic Coefficients of Friction of Plastic Film and Sheeting*. (2018). doi:10.1520/D1894-14.2
 24. Vu, I. Q. Fracture and Friction Characterization of Polymer Interfaces Fracture and Friction Characterization of Polymer Interfaces (Master's Thesis). (Virginia Polytechnic Institute and State University, 2015).
 25. Ten Thije, R. H. W., Akkerman, R., Ubbink, M. & Van Der Meer, L. A lubrication approach to friction in thermoplastic composites forming processes. *Compos. Part A Appl. Sci. Manuf.* **42**, 950–960 (2011).
 26. Fiber, G. & Composites, P. Thermoforming-stamping of Continuous Glass Fiber/Polypropylene Composites: Interlaminar and Tool–Laminate Shear Properties. *Thermoplast. Compos. Mater.* **17**, 137–165 (2004).
 27. Orczyca, J. E. L. G., Herwood, J. A. A. S., Iu, L. U. L. & Hen, J. U. C. Modeling of Friction and Shear in Thermoforming of Composites – Part I. *Compos. Mater.* **38**, (2004).
 28. Bian, X. X. *et al.* Effects of Processing Parameters on the Forming Quality of C-Shaped Thermosetting Composite Laminates in Hot Diaphragm Forming Process. *Appl Compos Mater* **20**, 927–945 (2013).
 29. Twigg, G. & Poursartip, A. An experimental method for quantifying tool – part shear interaction during composites processing. *Compos. Sci. Technol.* **63**, 1985–2002 (2003).
 30. Ersoy, N., Potter, K., Wisnom, M. R. & Clegg, M. J. An experimental method to study the frictional processes during composites manufacturing. *Compos. Part A* **36**, 1536–1544 (2005).
 31. Haanappel, S. P., Thije, R. H. W., Sachs, U., Rietman, B. & Akkerman, R. Formability analyses of uni-directional and textile reinforced thermoplastics. *Compos. Part A* **56**, 80–

- 92 (2014).
32. Fetfatsidis, K. A., Jauffrès, D., Sherwood, J. A. & Chen, J. Characterization of the tool / fabric and fabric / fabric friction for woven-fabric composites during the thermostamping process. *Int. J. Mater. Form.* **13** (2011). doi:10.1007/s12289-011-1072-5
 33. Brostow, W., Cassidy, P. E., Hagg, H. E., Jaklewicz, M. & Montemartini, P. E. Fluoropolymer addition to an epoxy : phase inversion and tribological properties. *Polymer (Guildf)*. **42**, 7971–7977 (2001).
 34. Sun, J., Li, M., Gu, Y., Zhang, D. & Li, Y. Interply friction of carbon fiber / epoxy prepreg stacks under different processing conditions. *J. Compos. Mater.* **48(5)**, 565–526 (2014).
 35. Kavehpour, H. P. & McKinley, G. H. Tribo-rheometry: From gap-dependent rheology to tribology. *Tribol. Lett.* **17**, 327–335 (2004).
 36. Gillham, J. K. Formation and Properties of Thermosetting and High Tg Polymeric Materials. *Polym. Eng. Sci.* **26**, 1429–1433 (1986).
 37. Mounif, E., Bellenger, V. & Tcharkhtchi, A. Time – Temperature-Transformation (TTT) Diagram of the Isothermal Crosslinking of an Epoxy / Amine System : Curing Kinetics and Chemorheology. *J. Appl. Polym. Sci.* **108**, 2908–2916 (2008).
 38. Franck, A. J. & Instruments, T. A. Understanding Rheology of Thermosets.
 39. Macosko, C. W. Rheological changes during crosslinking. *Br. Polym. J.* **17**, 239–245 (1985).
 40. Domínguez, J. C., Alonso, M. V, Oliet, M. & Rodríguez, F. Chemorheological study of the curing kinetics of a phenolic resol resin gelled. *Eur. Polym. J.* **46**, 50–57 (2010).
 41. Garschke, C., Parlevliet, P. P., Weimer, C. & Fox, B. L. Cure kinetics and viscosity modelling of a high-performance epoxy resin film. *Polym. Test.* **32**, 150–157 (2013).
 42. Roller, M. . Rheology of Curing Thermosets: A Review. *Polym. Eng. Sci.* **26**, 432–440 (1986).
 43. Halley, P. J. & Mackay, M. E. Chemorheology of Thermosets- An Overview. *Polym. Eng. Sci.* **36**, 593–609 (1996).
 44. Malkin, A. Y., Bolgov, S. A., Begishev, V. P. & Mansurov, V. A. Evolution of viscoelastic properties of polyurethane in the course of curing. *Rheol. Acta* **350**, 345–350 (1992).
 45. Apicella, A., Kenny, J., Nicolais, L. & Iannone, M. The Influence of Prepreg Ageing on the Chemorheology of Carbon Fibre Laminate Processing. *Compos. Struct.* 230–240 (1987).
 46. Miller, S. G. *et al.* Out-life characteristics of IM7/977-3 composites. *Int. SAMPE Tech. Conf.* (2010).
 47. Hexcel Corporation. *HexPly® M77 80°C-160°C Curing Epoxy Matrix Product Data*

- Sheet*. (2016).
48. Anton Parr GmbH. *Temperature Control for MCR Rheometers*. (2018).
 49. Schramm, G. A Practical Approach to Rheology and Rheometry. *Rheology* 291 (1994). doi:10.1017/CBO9781107415324.004
 50. TA Instruments. in *Testing an Unknown Material Using a Rheometer* 1–6 (2012).
 51. TA Instruments. in *Understanding rheology of structured fluids* 1–11 (2004).
 52. Corbridge, D. M., Harper, L. T., De Focatiis, D. S. A. & Warrior, N. A. Compression moulding of composites with hybrid fibre architectures. *Compos. Part A Appl. Sci. Manuf.* **95**, 87–99 (2017).
 53. Brostow, W. & Glass, N. M. Cure progress in epoxy systems : dependence on temperature and time. *Mater. Res. Innov.* **7**, 125–132 (2003).
 54. Yu, H., Mhaisalkar, S. G., Wong, E. H. & Khoo, G. Y. Time – temperature transformation (TTT) cure diagram of a fast cure non-conductive adhesive. *Thin Solid Films* **504**, 331–335 (2006).
 55. Sun, L. Thermal Rheological Analysis of Cure Process of Epoxy Prepeg. (Louisiana State University, 2002).
 56. Habibi, M. H. Effects of Out-Time on Cure Kinetics and Rheological Properties of Out-of-Autoclave and Autoclave Prepregs. (Wichita State University, 2013).
 57. Han, S. *et al.* Characterization of the rheological properties of a fast-curing epoxy-molding compound. *J. Rheol. (N. Y. N. Y.)* **41**, 177–195 (1997).
 58. Winter, H. H. Can the Gel Point of a Cross-linking Polymer Be Detected by the G' -G'' Crossover? *Polym. Eng. Sci.* **27**, 1698–1702 (1987).
 59. Bowden, F. P. & David, T. *Friction An Introduction to Tribology*. (Heinemann Educational Books Ltd, 1973).
 60. ASTM International. *ASTM D7780-12 Standard Test Method for Cure Behavior of Thermosetting Resins by Dynamic Mechanical Procedures using an Encapsulated Specimen*. (2017). doi:10.1520/D7750-12R17.2
 61. Shaghghi, S., Beheshty, M. & Rahimi, H. Preparation and Rheological Characterization of Phenolic/Glass Prepregs. *Iran. Polym. J.* **20**, 969–977 (2011).
 62. Agoda-Tandjawa, G. *et al.* Rheological characterization of microfibrillated cellulose suspensions after freezing. *Carbohydr. Polym.* **80**, 677–686 (2010).
 63. Rj, H. & Jm, T. Characterizing Rheological Cure Behavior of Epoxy Composite Materials. *J. Compos. Technol. Res.* **2**, 11–14 (1980).
 64. Lam, R. C. & Kardos, J. L. The Permeability and Compressibility of Aligned and Cross-Plied Carbon Fiber Beds During Processing of Composites. *Polym. Eng. Sci.* **31**, 1064–1070 (1991).

65. Potter, K. D. Understanding the origins of defects and variability in composites manufacture. *17 th Int. Conf. Compos. Mater.* 27–31 (2009).
66. Persson, B. *Sliding Friction: Physical Principles and Applications*. (Springer-Verlag, 2000).
67. Lucchetta, G., Marinello, F. & Bariani, P. F. Aluminum sheet surface roughness correlation with adhesion in polymer metal hybrid overmolding. *CIRP Ann. Manuf. Technol.* **60**, 559–562 (2011).
68. Sinha, S. K. & Briscoe, B. J. *Polymer Tribology*. (Imperial College Press, 2009).
69. Dowson, D. *et al. Thinning Films and Tribological Interfaces*. (2000).
70. Tuononen, A. J. Onset of frictional sliding of rubber – glass contact under dry and lubricated conditions. *Nat. Publ. Gr.* 1–10 (2016). doi:10.1038/srep27951
71. Dealy, J. M. & Saucier, P. C. *Rheology in Plastics Quality Control*. (2000).

Appendix A

Determination of Linear Viscoelastic Region and Effects of Sample Shape and Adhesive Type on Rheological Properties of HexPly M77 UD Prepreg

The objectives of the results in this section are to determine the linear viscoelastic region (LVE) of the prepreg, examine the effects of various set up such as prepreg shape and adhesive types on subsequent rheological behavior of the sample, and to establish a base experimental procedure for further testing.

A.1 Material and Methods

A.1.1 Material

The material studied in this work was HexPly® unidirectional (UD) prepreg (M77/38%/UD300/SGL-50K), supplied by Hexcel, Duxford, UK. The material is a 50K high strength carbon fiber tow, with a fiber areal density of 300 gsm, pre-impregnated with M77 epoxy resin (38% resin content).⁴⁷

A.1.2 Sample Preparation

The prepreg fabric was moved to room temperature at approximately 22°C before cutting into 28x28mm square samples with scissors, or into ~ 26mm circular samples with a stamping die and press (e.g. circular cutter, punch part XS819017, Cascav tools).

A.1.3 Rheological Measurements

Samples were loaded onto the bottom plate of the geometry with fiber orientation parallel to the machine, without adhesives, or are fixed to the bottom geometry with double sided pressure sensitive adhesive (PSA) (3M®), or cyanoacrylate (MXBON®). Sample adhesives (cyanoacrylate) were used for the LVE measurements. A 1mm ring geometry is used, and the top

and bottom geometry were cleaned after each experiment with acetone to remove residual epoxy transferred between tests.

Rheological measurements are conducted in dynamic oscillatory mode (strain sweep) with strain from 0.1% to 100% at a frequency of 1 hz, at ambient temperature to determine the linear viscoelastic region (LVE) of the sample.⁷¹

A.2 Results and Discussion

A.2.1. Determination of LVE and Effects of Prepreg Shape on Rheological Properties

Prepreg samples are often cut into specific shapes with precise dimensions (e.g. square or circular) to minimize variabilities between rheological measurements.^{5,24,46} The effects of sample shape on the rheological response of samples are examined by conducting oscillatory strain sweep experiments at ambient temperature, with a strain (%) from 0.01-100%, a normal force of 20N and 30N (for the square and circular sample, respectively), and a frequency of 1 hz. The plots of storage modulus (G') and loss modulus (G'') vs. shear strain [%] of the square and circular sample are shown in Figure A.2.

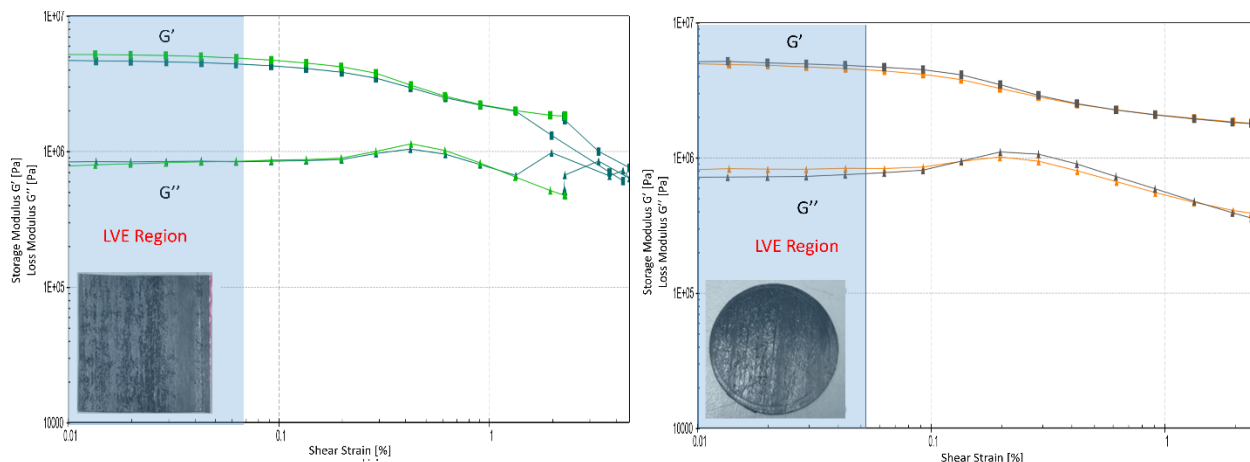


Figure A.2. Storage and Loss Modulus vs. Shear strain (%) of square (L) and circular (R) samples measure with 1mm ring geometry under SAOS mode, ambient temperature, 0.01-100 strain %, 20 and 30 N (respectively)

The overlapping values of the samples suggest the experiments are both repeatable regardless of sample shape. The linear viscoelastic region (LVE) for the square sample is observed at below 0.07% strain. A lower LVE range, with a maximum of 0.05% strain, is observed for the circular sample. The result suggests that circular samples would be more sensitive to frequency change due to the lower LVE range. However, it should be noted that the lower LVE range of the circular sample could be due to the larger normal force applied during the experiments.

A more important parameter to consider is the drastic change in G' and G'' of the square samples at above 1% strain, suggesting significant structural instability as strain increases. This behavior could be caused by the presence of excess fabric of the square sample (e.g. “edge effect”). A comparison of the square and circular sample loaded in the test fixture is shown in Figure A.3. While this large change in G' and G'' could be of concern, the fact that the behavior occurs at a region above the LVE suggests that this might not be as much of an issue as long as subsequent experiments are conducted below the LVE limit.

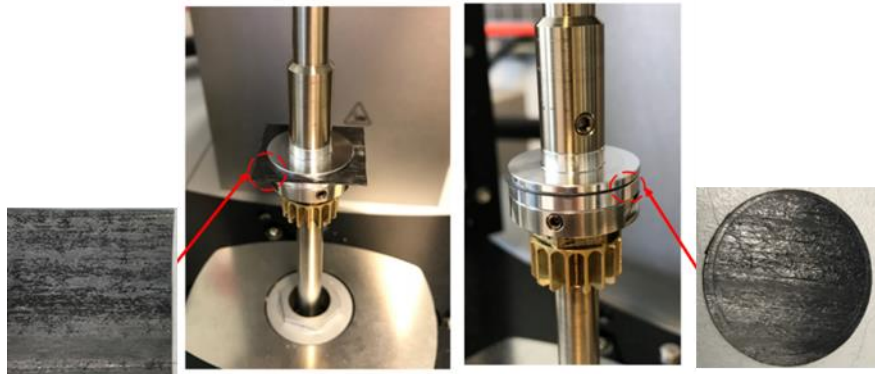


Figure A.3. Prepreg in fixture (left) square sample with excess fabric, and (right) circular sample

While the circular sample seems to be a more “stable” choice for our tests, split propagation in the fiber direction is often observed during the cutting process with the circular punch (Figure A.4).



Figure A.4. Split circular sample from cutting process

Since sample splitting was not observed during the cutting process of square samples, and the rheological results suggests relatively good repeatability and stability below the LVE region, subsequent tests were conducted similar to the reported experimental conditions below 0.07% strain. It should be noted that the square sample dimensions are less consistent since samples are measured and cut with scissors by hand, compared to a circular punch/die.

A.2.2 Effect of Sample Adhesive Type on Rheological Properties

In addition to controlling sample shape and size, specimens should be held firmly in place during experiments to minimize fabric twist/overlap. Rheological tests with preregs have been conducted with multiple layers of prepreg, using double sided tape or cyanoacrylate as an adhesive.^{5,24,46} The goal of the present experiment is to ensure slippage occurs only at the top of the plate between the geometry and prepreg to mimic tool-ply friction. A schematic of the adhesive test set up is show in Figure A.5.

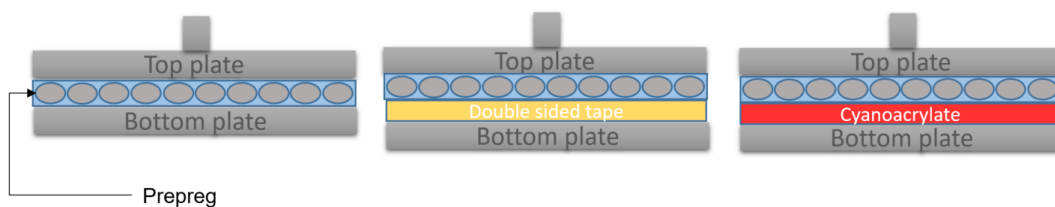


Figure A.5. Schematic of sample set up for adhesive tests

A set of steady shear tests were conducted with an angular deflection from 0-100mrad, at ambient conditions, with a normal force of 5N, and 1mm ring geometry to examine the effects of sample adhesive on measured rheological properties. The result of the experiments are shown in Figure A.6. The sample without adhesive reached the rheometer torque limit of 0.2 N·m, whereas the PSA exhibited a continuous sliding behavior, and the sample with the cyanoacrylate adhesive showed a plateau and constant torque over the deflection range.

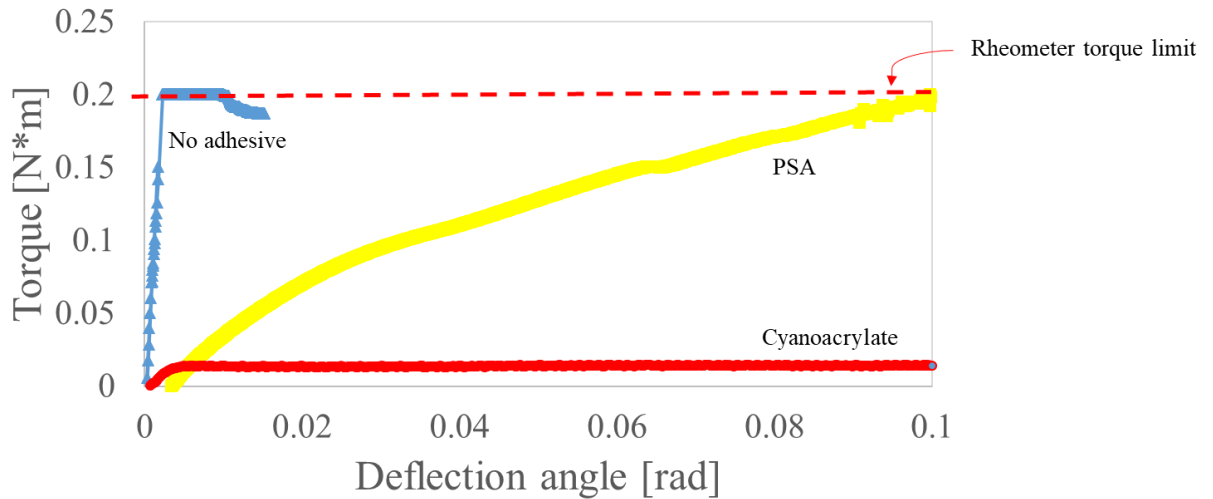


Figure A.6. Torque vs. deflection result of samples with/without sample adhesives

Variations in the experimental results can be explained by the different slip location/deformation mechanism between the surfaces as shown in Figure A.7.

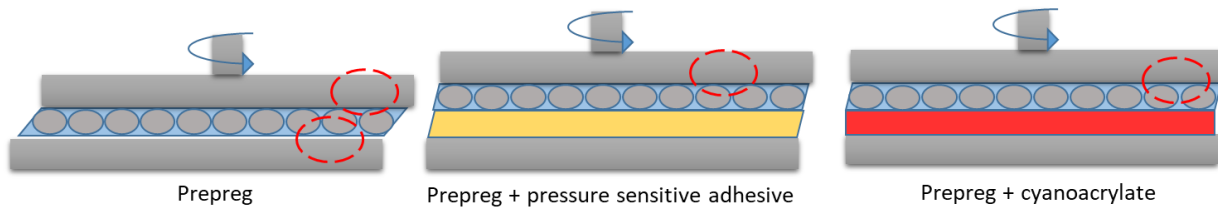


Figure A.7. Proposed slip location (red circles) and deformation mechanisms between sample and geometry during steady shear

Since the uncured prepreg is somewhat soft/flexible at room temperature, the rotating motion of the top geometry could cause the fabric to move or even twist at either the top or bottom plate,

resulting in the large increase in torque at low deflection angles. Although the presence of PSA improves the prepreg-plate contact at the bottom geometry, the continuous sliding behavior observed over the deflection interval suggests that there is still some deformation/movement from both the prepreg and PSA. In addition, since PSA is a viscoelastic material, changes in sample viscoelastic properties could occur at different experimental temperatures. Since cyanoacrylate is a thermosetting polymer, the strong adhesive force between the prepreg and cyanoacrylate would prevent slip at the bottom geometry, and reduce movement/deformation of the prepreg.

A.3 Conclusion

The effects of sample shape and adhesive type on the rheological response of samples were examined by a parallel plate rheometer (modified 1mm ring geometry) at ambient temperatures. Oscillatory strain sweep results suggest relatively good repeatability and stability below the LVE region for both square and circular samples. Subsequent tests were conducted with square samples due to challenges with cutting circular samples at experimental conditions below 0.07% strain. The LVE of the material should be examined at a wider set of temperatures to verify that the material is within the LVE region at higher temperatures during SAOS tests. The excess fabric could cause an effective increase in measured results due the “edge effect” (e.g. more resistance to motion from the excess fabric). Steady shear results suggest that prepreg movement/distortions between the geometry can be reduced in the presence of an adhesive. A continuous movement of PSA-prepreg system is observed in steady shear experiments due to the viscoelastic property of PSA, whereas minimal movement of the prepreg is observed in the cyanoacrylate-prepreg system due to the strong adhesion force formed between the prepreg-cured cyanoacrylate-bottom geometry.

Appendix B

Effects of Surface Roughness and Dwell time on Frictional Sliding Tests

A common challenge with testing carbon fiber epoxy prepregs are the difficulties in sample reproducibility due to variations in bulk properties of the as received material.⁵³ A cut section of the as received prepreg is shown in Figure B.1, with an uneven distribution of epoxy across the surface of the prepreg. Since the rheological behavior of the prepreg is dependent on both the carbon fiber and epoxy matrix, the varied epoxy surface coverage will likely cause differences in measured results. As such, it was important to keep track of sample location (such as row) for subsequent tests.

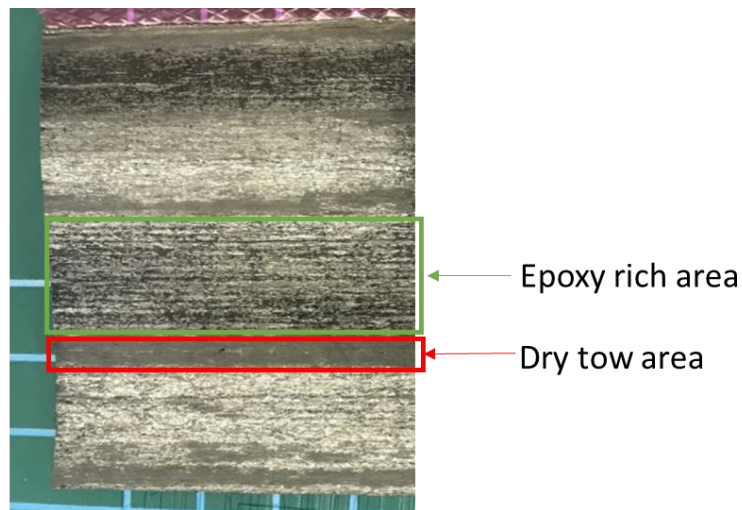


Figure B.1. As received prepreg (HexPly M77/38%/UD300/50K) before cutting, illustrating varied resin coverage across surface (120 x 90 mm shown)

B.1 Material and Methods

B.1.1 Material

The material studied in this work was HexPly® unidirectional (UD) prepreg (M77/38%/UD300/SGL-50K), supplied by Hexcel, Duxford, UK. The material is a 50K high strength carbon fiber tow, with a fiber areal density of 300 gsm, pre-impregnated with M77 epoxy resin (38% resin content).⁴⁷

B.1.2 Sample Preparation

The prepreg fabric is thawed to room temperature at approximately 22°C before cutting into 28x28mm square samples.

B.1.3 Rheological measurements

Samples were loaded onto the bottom geometry with fiber orientation parallel to the machine and were fixed to the bottom geometry with cyanoacrylate (MXBON®). A 1mm ring geometry is used, and the top and bottom geometry were cleaned after each experiment with acetone to remove residual epoxy transferred between tests.

Steady shear rheological measurements were conducted at sliding velocity of 0.1rad/s at 20°C and a normal force of 5N.

B.1.4 Sample staging

The pre-cut prepreg (28x28 mm) were placed on aluminum foil and tray into an universal oven (Mettler UF75) at room temperature. The oven is heated at 10°C/min to 90°C and cured for 180 minutes before removing from oven to room temperature for the “fast cool” samples, and cooled at a rate of 4.2°C/min for 10 minutes (by opening the oven door with approx. 2 in slit) before removing sample to ambient temperature (“slow cool” samples).

B.2 Results and Discussion

B.2.1 Repeatability of Uncured Samples

Sample repeatability of uncured prepreg was examined for three uncured samples using a 1mm annulus and a sliding velocity of 0.1rad/s at 20°C and a normal force of 5N. Variability between samples are observed (Figure B.2). The static friction of uncured sample 3 is much

larger compared to sample 1 and sample 2, where it reaches the torque limit of the machine. The kinetic friction of sample 3 is much lower than the value measured for sample 1 and sample 2.

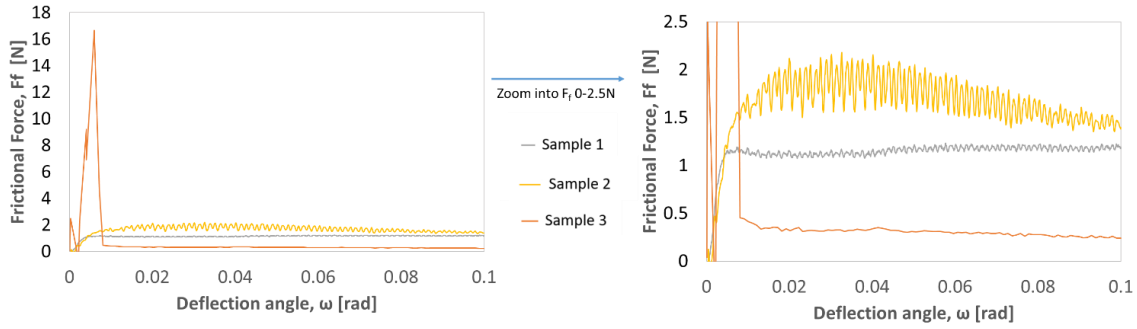


Figure B.2. Frictional force and gap height vs. deflection angle of uncured samples at 20°C, 0.1 rad/s, 5N

A more detailed result of differences between the three samples are shown in Table B.1. The most noticeable differences between the samples are the variations in experimental temperature, gap change, dwell time (t_0).

Table B.1. Frictional sliding results of uncured samples at 20°C, 0.1rad/s, 5N

Sample	Temp. [°C]	F_s [N]	F_k [N]	h_0 [mm]	Gap change [mm]	t_0 [s]	Row [-]	Environmental chamber?	Humidity [%]
1	22	1.23	1.12	0.399	-0.014	600	5	No	49
2	21	2.17	1.69	0.393	-0.010	600	5	No	50
3	20	16.66	0.30	0.330	-0.001	829	9	Yes	(low)

The viscoelastic properties of a sample corresponding to the experimental temperatures are shown in Table B.2, where a higher experimental temperature corresponds to a lower viscosity. While a decrease in effective F_k generally corresponds to increasing temperature (due the decrease in matrix viscosity⁵). An increase in F_k is observed with increase in temperature for the samples tested. In addition, an increase in $\tan \delta$ was observed with increasing experimental temperature, which suggests that the sample will behave more like an elastic solid at the lower temperature compared to samples at higher temperatures. Such behavior could explain why there

is a larger change in gap height at the higher temperatures, as a higher $\tan \delta$ would allow more movement of the tool closer to the fiber surface, resulting in fiber-tool interaction and an effective increase in F_f .⁵

Table B.2. Viscoelastic properties measured from SAOS at 0.05% strain, 1hz, heating rate of 10°C

Sample	T [°C]	η^* [Pa·s]	$\tan \delta$ [-]	h_0 [mm]	dh [mm]
1	21.8	$8.9 \cdot 10^5$	0.29	0.382	0
2	21.3	$9.21 \cdot 10^5$	0.25	0.383	0.001
3	20.0	$9.88 \cdot 10^5$	0.16	0.383	0.001

While differences in experimental temperature could explain the changes in gap height observed in the samples, a more plausible reason for the difference in measured response is likely due to variations in epoxy coverage between sample rows (see Figure B.3). Sample 3 from row 9 has more dried tow area compared to sample 1 and 2 from row 5, which could explain the low F_k of sample 3 compared sample 1 and 2.

In general, static friction is considered as friction between non-moving surfaces, and is dominated by adhesion between the contact surface asperities, the time and mode of contact, whereas the kinetic friction is described by the friction between two moving surfaces and is dominated by the viscoelastic properties of the materials.⁵ As such, the large F_s of sample 3 compared to sample 1 and 2 could be attributed to the longer initial contact time, t_0 of the tool-ply prior to the start of the experiment. Another possible reason for the large differences in F_s could be the lower humidity provided by the constant air flow of the cooling chamber, versus the higher humidity at ambient conditions. At ambient conditions, the humidity is much higher (approximately 50%) compared to experiments conducted at 20°C or heated conditions. Therefore, materials are typically characterized with the use of the environmental chamber to reduce the variations in humidity.

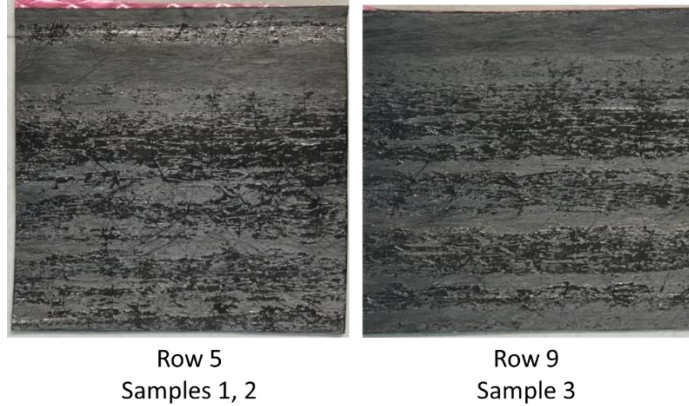


Figure B.3. cut prepreg with varied resin coverage between rows (28 x 28mm squares)

B.2.2 Repeatability of Cured samples

In theory, cured sample should have less variation in the gap between the geometry plates as the cured prepreg would have limited movement (due to much adhesion contribution, and the friction behavior should be similar to solid-solid surfaces). Sample repeatability of cured prepreg was examined for three oven cured samples using a 1mm annulus and a sliding velocity of 1 mrad/s at 22°C and a normal force of 5N. The results are shown in Figure B.4.

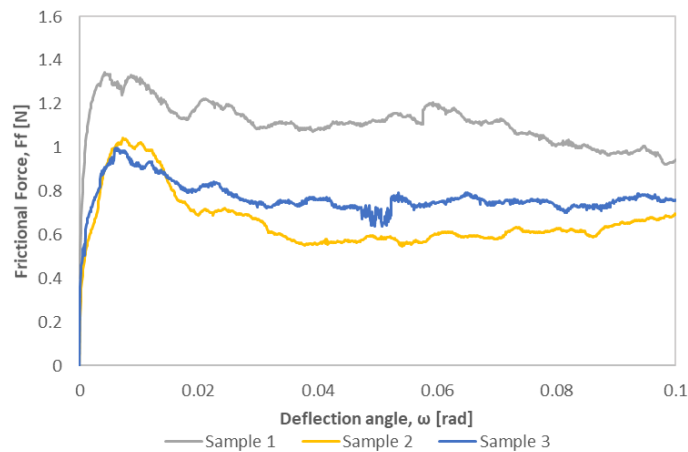


Figure B.4. Frictional force vs. deflection angle of cured samples from row 5 at 22°C, 1 mrad/s, 5N

It should be noted that audible cracking sounds were emitted from the samples when removing from the oven and while cooling from curing temperature to ambient temperature.

Uneven surfaces were observed for the samples cooled at a fast cooling rate compared to samples cooled at a slow rate (Figure B.5).

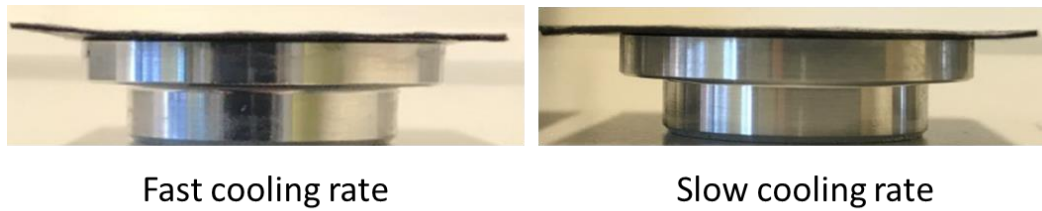


Figure B.5. Variation in surface smoothness of cured prepreg samples made from different cooling rates (L) fast cooling rate (R) and slow cooling rate

A detailed comparison of the frictional sliding results of the “fast cooled” and “slow cooled” samples are shown in Table B.3. An overall higher value of F_f is observed for the “slow cooled” sample, where the smoother surface could promote tool-laminate contact (higher contact area) resulting in the larger F_f observed. However, due to the limited sample size and qualitative nature of this work, additional experiments are required to verify the effects of the surface roughness on sample repeatability.

Table B.3. Frictional sliding results of cured samples at 22°C, 0.1 rad/s, 5N

Sample	Cooling rate	Temperature [°C]	F_s [N]	F_k [N]	h_0 [mm]	Δh [mm]	t_0 [s]
1	Slow	22	1.35	1.07	0.418	-0.001	300
2	Fast	22	1.05	0.62	0.402	-0.003	300
3	Fast	22	1.00	0.75	0.410	-0.006	300

B.3 Conclusion

Due to variability of epoxy on the as received prepreg, sample repeatability was examined for uncured and cured samples at 20°C. Variations in experimental temperature of the uncured samples were observed due to the use of a cooling chamber (for sample 3, 20°C) compared to samples conducted at ambient conditions (for sample 1 21.8°C and 2, 21.3°C). For

the uncured samples, the kinetic friction force seems to be dependent on the experimental temperature, and epoxy coverage where an increase in experimental temperature (and in extension, epoxy viscosity) resulted in an unexpected increase in F_k value.

The relative viscoelastic properties of the samples were compared by examining the SAOS result of a sample (0.05% strain, 1 hz, 10°C/min). The $\tan \delta$ of the sample increased with increase with experimental temperature, along with a larger change in gap height, suggesting that the variability between the uncured samples could be the result of increased frictional resistance from the matrix fiber at the lower gap height. The large F_s of sample 3 (at the low temperature) could be a combination of longer initial contact time (adhesion contribution), whereas the low F_k (about 1/5 of the value compared to the other) could be a contribution of low frictional resistance from the dry tow area, and the low relative humidity from the cooling chamber.

Sliding friction of cured samples was examined to determine sample repeatability (assuming minimal deformation and adhesion contributions will occur from the cured epoxy). Changes in surface roughness were observed depending on the cooling rate after cure, where the sample cooled at a faster rate had a rougher surface. Higher friction forces were observed for the slow-cooled sample due to the larger contact area available (smoother surface).

It should be noted that the observed surface variations are qualitative in nature, but the overall behavior suggest that the repeatability of the samples depends highly on the surface variations (such as epoxy coverage, and surface smoothness). In addition, we should expect the cured samples to have similar F_f at higher initial contact times since the cured samples should not have “tack” compared to uncured samples.

The overall results suggests that frictional behaviors at low temperatures is dependent on surface variability of the as received prepreg. As materials with less epoxy coverage (higher dry

tow area) would exhibit higher frictional values due to the absence of resin between the surfaces, compared to a region with a higher epoxy coverage, which would exhibit frictional behavior in the BL with lower frictional values. Future work should include examining the average resin distribution per unit area of the as received prepreg to account for the overall frictional effect of the dry tow/normal epoxy coverage areas.